Ecological Monographs, 71(2), 2001, pp. 277–303

ESTIMATING CHAOS AND COMPLEX DYNAMICS IN AN INSECT POPULATION

BRIAN DENNIS,[1,6] ROBERT A. DESHARNAIS,[2] J. M. CUSHING,[3] SHANDELLE M. HENSON,[4] AND R. F. COSTANTINO[5]

[1]*Department of Fish and Wildlife Resources and Division of Statistics, University of Idaho, Moscow, Idaho 83844 USA*
[2]*Department of Biology and Microbiology, California State University, Los Angeles, California 90032 USA*
[3]*Department of Mathematics, Interdisciplinary Program in Applied Mathematics, University of Arizona, Tucson, Arizona 85721 USA*
[4]*Department of Mathematics, College of William and Mary, Williamsburg, Virginia 23187 USA*
[5]*Department of Biological Sciences, University of Rhode Island, Kingston, Rhode Island 02881 USA*

Abstract. A defining hypothesis of theoretical ecology during the past century has been that population fluctuations might largely be explained by relatively low-dimensional, nonlinear ecological interactions, provided such interactions could be correctly identified and modeled. The realization in recent decades that such nonlinear interactions might result in chaos and other exotic dynamic behaviors has been exciting but tantalizing, in that attributing the fluctuations of a particular real population to the complex dynamics of a particular mathematical model has proved to be an elusive goal. We experimentally tested a model-predicted sequence of transitions (bifurcations) in the dynamic behavior of a population from stable equilibria to quasiperiodic and periodic cycles to chaos to three-cycles using cultures of the flour beetle *Tribolium*. The predictions arose from a system of difference equations (the LPA model) describing the nonlinear life-stage interactions, predominantly cannibalism. We built a stochastic version of the model incorporating demographic variability and obtained conditional least-squares estimates for the model parameters. We generated 2000 ''bootstrapped data sets'' with a time-series bootstrap technique, and for each set we reestimated the model parameters. The resulting 2000 bootstrapped parameter vectors were used to obtain confidence intervals for the model parameters and estimated distributions of the Liapunov exponents for the deterministic portion (the skeleton) of the model as well as for the full stochastic model. Frequency distributions of estimated dynamic behaviors of the skeleton at each experimental treatment were produced. For one treatment, over 83% of the bootstrapped parameter estimates corresponded to chaotic attractors, and the remainder of the estimates yielded high-period cycles. The low-dimensional skeleton accounted for at least 90% of the variability in the population abundances and accurately described the responses of populations to experimental demographic manipulations, including treatments for which the predicted dynamic behavior was chaos. Demographic stochasticity described the remaining noise quite well. We conclude that the fluctuations of experimental flour beetle populations are explained largely by known nonlinear forces involving cannibalistic-stage interactions. Claims of dynamic behavior such as periodic cycles or chaos must be accompanied by a consideration of the reliability of the estimated parameters and a realization that the population fluctuations are a blend of deterministic forces and stochastic events.

Key words: bifurcations in dynamic behavior; bootstrap parameter estimates; chaos; complex dynamics; Liapunov exponents; mathematical modeling; periodic cycles; population dynamics, chaotic; population dynamics, nonlinear; population model parameters, estimating; quasiperiodicity; Tribolium.

INTRODUCTION

Nonlinear theory in ecology can be summarized as a broad hypothesis: that the fluctuation patterns of abundances in many population systems are explained largely by relatively low-dimensional nonlinear interactions. Population fluctuations in this view are the result of stable points, stable periodic and aperiodic cycles, chaos, stable and unstable manifolds of invariant sets, and multiple attractors, with the addition of some unexplained noise. Some recent applications of nonlinear modeling in ecology have met with encouraging success, due in part to improved statistical methods and stochastic modeling approaches (Costantino et al. 1995, 1997, 1998, Dennis et al. 1995, 1997, Ellner and Turchin 1995, Begon et al. 1996, Stenseth et al. 1996, Higgens et al. 1997, Leirs et al. 1997, Bjornstad et al. 1998, Cushing et al. 1998*a*, *b*, Finkenstadt et al. 1998, Dixon et al. 1999, Henson et al. 1999).

One particular aspect of nonlinear dynamic theory—

Manuscript received 24 June 1999; revised 3 February 2000; accepted 20 February 2000; final version received 27 March 2000.

[6] E-mail: brian@uidaho.edu

chaos—provides an unusual and intuitively unexpected prediction of population behavior: low-dimensional *deterministic* forces can cause apparently random fluctuations in population abundances. It was therefore not surprising that the recognition of chaotic dynamics in ecological models (May 1974*a*, May and Oster 1976) was followed immediately by the search for chaos in existing population time-series data (Hassell et al. 1976). Although a few researchers did conduct field studies to test chaotic predictions (see Tilman and Wedin 1991), the dominant focus over the next two decades continued to be on historical data sets. Connecting nonlinear theory to observed population fluctuations proved to be a formidable challenge (Schaffer 1984, Olsen et al. 1988, Pool 1989*a, b*, Olsen and Schaffer 1990, Ellner 1991, Hastings et al. 1993, Grenfell et al. 1994). Indeed, the lack of data has limited progress. While the search for chaos as an explanation of population time series continues, the inquiry has stimulated new explanations of data, the development of new procedures for data analysis (Schaffer 1984, Olsen et al. 1988, Bartlett 1990, Hassell et al. 1991, Logan and Hain 1991, Nychka et al. 1992, Turchin and Taylor 1992, Ascioti et al. 1993, Godfray and Grenfell 1993, Turchin 1993, 1995, Chan and Tong 1994, Ellner and Turchin 1995, Falck et al. 1995*a, b*, Desharnais et al. 1997, Perry et al. 1997), and a new phase of experimental population research (Kareiva 1995, Godfray and Hassell 1997, Rohani and Earn 1997, Cipra 1999, Kendall et al. 1999, Zimmer 1999).

The complexity of the natural systems involved in the historical data sets, along with the inherent difficulties in confidently linking such systems with theory, pointed to the need for controlled laboratory experiments—experiments designed and analyzed with the specific intention of testing the predictions of nonlinear population theory. Although laboratory microcosms are no substitute for field experiments, they are useful for testing basic ecological concepts (Kareiva 1989, Godfray and Blythe 1990, Begon et al. 1996, Ives et al. 1996, Bjornstad et al. 1998, Finkenstadt et al. 1998, Miramontes and Rohani 1998). In this paper we report on experimental evidence of chaos and other complex dynamic behaviors obtained in such a laboratory experiment. A brief announcement of these results appeared in Costantino et al. (1997); we now provide a complete description of our experiment and data as well as new, extended analyses. An overview of our research effort on nonlinear dynamics is given by Cushing et al. (1996, 1998*a*, 2001).

Nonlinear theory often predicts transitions in the long-term dynamics of a population in response to changing parameter values. For example, the familiar one-dimensional, discrete-time logistic model forecasts dynamical changes (bifurcations) from extinction to equilibrium to two-, four-, eight-cycles, etc., to chaos as the birthrate parameter is increased (May 1974*a*). We view such a predicted sequence of transitions as a hypothesis subject to experimental scrutiny in the laboratory. The idea for a ''transitions experiment'' is straightforward: manipulate biological parameters (such as the birthrate) in order to document experimentally the model-predicted transitions among dynamic states.

There is a demanding prerequisite for both positing and testing a transitions hypothesis: the identification of an adequate mathematical model. Our work began with the derivation of a biologically based stage-structured model (the larva–pupa–adult or ''LPA'' model) for the flour beetle *Tribolium castaneum* Herbst (Dennis et al. 1995). We applied this model to the data of Desharnais and Costantino (1980) and, with diagnostic analyses of time-series residuals, showed that the LPA model did an excellent job of predicting responses to the experimental perturbations in population stage structure (Dennis et al. 1995). More recently, Benoît et al. (1998) conducted a set of manipulation experiments using the species *T. confusum* that provided an independent validation of the LPA model.

Following the documentation of the LPA model, we conducted two long-term transitions experiments. In the first transitions experiment, we manipulated the adult mortality rates in beetle cultures and observed transitional changes in the population dynamics corresponding to the bifurcations predicted by the mathematical model (Costantino et al. 1995, Dennis et al. 1997). Maximum-likelihood parameter estimates were obtained, 95% confidence intervals were calculated from profile likelihoods, and the variance–covariance matrices for both the control and treatment replicates were presented. The LPA model did not forecast chaotic attractors in this experiment, and none were observed experimentally (Rohani and Miramontes 1996, Dennis et al. 1997). The model-predicted transitions in population dynamics from equilibria to periodic cycles to aperiodic cycles were documented statistically in the data (Costantino et al. 1995, Dennis et al. 1997).

In this paper we present the results of the second transitions experiment, in which a model-predicted route to chaos was forecast. Our initial report of chaos (Costantino et al. 1997) was based on a point estimate of a set of parameters. What kind of confidence statement can be attached to such a report? Claims of chaos or even stable-point equilibria or stable cycles are typically subject to estimation error (Dennis et al. 1995, Falck et al. 1995*a, b*). However, it is difficult to produce and interpret confidence statements about dynamic behavior. Some approaches that have been used are profile likelihood methods (Dennis et al. 1995, Bailey et al. 1997), parametric bootstrapping methods (Dennis and Taper 1994), and semiparametric bootstrapping methods (Falck et al. 1995*a, b*). Of these methods, the semiparametric bootstrapping approach is theoretically more robust to misspecification of the noise distribution in the time-series model.

Our objective here is to explore the robustness of

the results of our second transitions experiment and to ascertain confidence levels for estimates of dynamic behavior. We begin by refitting the LPA model using a noise structure based on demographic stochasticity that describes the data more accurately than our original environmental noise structure (Costantino et al. 1997). We calculate parameter estimates for the stochastic model using the method of conditional least squares (Klimko and Nelson 1978, Tong 1990, Dennis et al. 1995). To calculate confidence intervals, we modify the semiparametric bootstrapping method used by Falck et al. (1995*a*, *b*). The estimated deterministic portion of the model is combined with a resampling of the model residual vectors to generate 2000 ''bootstrapped data sets.'' Model parameter vectors are estimated for each bootstrapped data set, and both deterministic and stochastic Liapunov exponents are computed for each combination of the 2000 bootstrapped parameter vectors and eight experimental treatments. With the 2000 bootstrapped parameter vectors we obtain frequency distributions of Liapunov exponents and frequencies of attractor types predicted by the deterministic portion of the model for each experimental treatment. We show that the flour beetle populations display an array of complex dynamic behaviors that includes a strong influence of chaos. We discuss the difference between the deterministic and the stochastic Liapunov exponents, and conclude that the stochastic Liapunov exponents probably should not be used as a benchmark of chaos. We caution that claims of ''dynamic behavior'' such as periodic cycles and chaos must be accompanied by a consideration of the reliability of the estimated parameters and a realization that the population fluctuations are a combination of the influence of the underlying deterministic dynamics as well as of stochastic events. We discuss the interplay of stochastic and deterministic forces (Bartlett 1990, Renshaw 1994), the meaning of chaos in a stochastic system, and the importance of incorporating stochastic forces along with studying and quantifying the influence of underlying deterministic forces in a population model.

Methods and Data

LPA model

Many species of *Tribolium* are cannibalistic (Park et al. 1965), including the species *Tribolium castaneum* (Herbst) used in this project. The LPA (larva–pupa–adult) model is built on the assumption that the nonlinear interactions among the life-cycle stages caused by cannibalism are the driving mechanisms of the dynamics for this species. The LPA model is a system of three difference equations that relate the numbers of animals at time t to the number of animals at time $t - 1$:

$$L_t = bA_{t-1}\exp(-c_{el}L_{t-1} - c_{ea}A_{t-1}) \quad (1)$$

$$P_t = L_{t-1}(1 - \mu_l) \quad (2)$$

$$A_t = P_{t-1}\exp(-c_{pa}A_{t-1}) + A_{t-1}(1 - \mu_a). \quad (3)$$

In this model formulation (Dennis et al. 1995, 1997), L_t is the number of feeding larvae (referred to as the ''L-stage''), P_t is the number of large larvae, non-feeding larvae, pupae, and callow adults (called the ''P-stage''), and A_t is the number of sexually mature adults (''A-stage animals'') at time t. The unit of time is 2 wk and is, approximately, the average amount of time spent in the feeding larval stage under our experimental conditions. The unit of time is also approximately the average duration of the P-stage. The quantity b is the number of larval recruits per adult per unit of time in the absence of cannibalism. The fractions μ_l and μ_a are the larval (l) and adult (a) rates of mortality, respectively, in one time unit. The exponential nonlinearities account for the cannibalism of eggs (e) by both larvae and adults and the cannibalism of pupae by adults. The fractions $\exp(-c_{el}L_{t-1})$ and $\exp(-c_{ea}A_{t-1})$ are the probabilities that an egg is not eaten in the presence of L_{t-1} larvae and A_{t-1} adults, respectively, in one time unit. The fraction $\exp(-c_{pa}A_{t-1})$ is the survival probability of a pupa (p) in the presence of A_{t-1} adults in one time unit. Eqs. 1–3 represent the deterministic population forces upon which we build our stochastic model.

Demographic variability

Different types of stochastic mechanisms produce different patterns of variability. In particular, two broad classes of stochastic mechanisms important to populations have been widely discussed: demographic stochasticity and environmental stochasticity (May 1974*b*, Shaffer 1981). In order to connect a deterministic population model with time-series data, the population model has to be converted into a stochastic model (Dennis et al. 1995). The types of stochastic mechanisms affecting the population therefore have to be carefully considered and formulated.

''Demographic stochasticity'' is the variability in population size caused by independent random contributions of births, deaths, and migrations by individual population members. Demographic stochasticity can be modeled by taking each individual's net contribution to the population in a unit of time to be the outcome of an independent, discrete random variable. A simple example is survival: an individual contributes ''0'' to the population in the next time unit with probability μ, where μ is the probability of death during the time unit, and ''1'' to the population with probability $1 - \mu$. If many individuals are members of a homogeneous cohort, then demographic events can often be aggregated analytically at the cohort level into a known probability distribution for cohort size at the next time unit.

For instance, suppose each member of a cohort of n_{t-1} individuals at time $t - 1$ has the same unit-time survival probability, $1 - \mu$. A deterministic model for the number of survivors at time t is $n_t = n_{t-1}(1 - \mu)$. If each cohort member were instead subjected independently to a simple, random survival process, the cohort at time t would be a random variable, N_t, with

a binomial(n_{t-1}, $(1 - \mu)$) distribution. Note that the binomial distribution for N_t is conditional on the attained value, $N_{t-1} = n_{t-1}$, of the previous cohort size. The conditional mean of N_t is $n_{t-1}(1 - \mu)$ (the deterministic expression), and the conditional variance of N_t is $n_{t-1}(1 - \mu)\mu$ (that is, the conditional variance is proportional to n_{t-1}).

We constructed a stochastic version of the LPA model containing demographic variability. In the stochastic version, we used the binomial and Poisson distributions to describe the aggregation of demographic events within the life stages. The simplest case is the P-stage model (Eq. 2). In the stochastic model, P_t is a random variable. The distribution of P_t given $L_{t-1} = l_{t-1}$ was taken to have a binomial(l_{t-1}, $(1 - \mu_l)$) distribution. The A-stage (Eq. 3) is the sum of two survival processes: recruits from the P-stage, denoted R_t, and surviving adults, denoted S_t. We assumed that R_t given $P_{t-1} = p_{t-1}$ and $A_{t-1} = a_{t-1}$ has a binomial(p_{t-1}, $\exp(-c_{pa}a_{t-1})$) distribution; the P-stage survival probability is the nonlinear function of a_{t-1} from Eq. 3. Also, S_t was assumed to have a binomial(a_{t-1}, $(1 - \mu_a)$) distribution.

The L-stage is a compound process: a random number of potential recruits is produced (with conditional mean ba_{t-1}), and each potential recruit subsequently undergoes a survival process in which the conditional survival probability, $\exp(-c_{el}l_{t-1} - c_{ea}a_{t-1})$, depends on the system state variables l_{t-1} and a_{t-1} (Eq. 1). We assumed that the number of potential recruits has a Poisson(ba_{t-1}) distribution (i.e., a Poisson distribution with mean ba_{t-1}), and that the number of subsequent survivors has a binomial distribution. An elementary property is that if a random variable Y has a binomial(n, p) distribution given $N = n$, and N has a Poisson(λ) distribution, then the resulting distribution for Y is Poisson($p\lambda$) (Boswell et al. 1979). Thus, the conditional distribution of L_t given $L_{t-1} = l_{t-1}$ and $A_{t-1} = a_{t-1}$ becomes a Poisson distribution with mean $ba_{t-1}\exp(-c_{el}l_{t-1} - c_{ea}a_{t-1})$.

Our stochastic demographic LPA model thus takes the conditional one-time-step distributions of L_t, P_t, and A_t to be independent, discrete probability distributions:

$$L_t \sim \text{Poisson}(ba_{t-1}\exp[-c_{el}l_{t-1} - c_{ea}a_{t-1}]) \quad (4)$$

$$P_t \sim \text{binomial}(l_{t-1}, (1 - \mu_l)) \quad (5)$$

$$R_t \sim \text{binomial}(p_{t-1}, \exp[-c_{pa}a_{t-1}]) \quad (6)$$

$$S_t \sim \text{binomial}(a_{t-1}, [1 - \mu_a]) \quad (7)$$

$$A_t = R_t + S_t. \quad (8)$$

Here ''$\sim$'' means ''is distributed as.''

For most statistical inferences reported in this paper, we undertook an additional modification of the stochastic demographic LPA model (Eqs. 4–8). We transformed the observations so that the stochastic demographic model would be approximated by a nonlinear autoregressive (NLAR) model. An NLAR model has the form

$$X_t = h(X_{t-1}) + E_t \quad (9)$$

where X_t is a state variable at time t, the function $h(\cdot)$ is the ''skeleton'' (underlying deterministic equation for X_t; Tong 1990), E_t is a normally distributed random variable with mean zero and variance σ^2, and E_1, E_2, . . . are uncorrelated. NLAR models have some advantages and conveniences for our analyses. First, parameter estimates retain a theoretical robustness to departures of the data from distributional assumptions (see *Parameter estimation*, below). Second, the numerically intensive calculations and simulations that we needed involve straightforward algorithms for least squares and normal random-variable generation. Finally, NLAR model evaluation can be based on familiar diagnostic methods using residuals (see Dennis et al. 1995).

The idea behind the NLAR approximation is to find a transformation, $X_t = g(N_t)$, where N_t is a state variable in the original model, for which the distribution of X_t given $X_{t-1} = x_{t-1}$ is approximately normal with a constant variance (that is, a variance that does not depend on x_{t-1}). If a variable N_t has a Poisson distribution with mean λ, then a well-known result from statistics is that $X_t = \sqrt{N_t}$ has approximately a normal distribution with a mean of $\sqrt{\lambda}$ and a constant variance that does not depend on the value of λ (Rao 1973). Thus, the square-root transformation stabilizes and normalizes the variance for the L-stage variable (Eq. 4). Also, the binomial distributions in the P-stage and A-stage models (Eqs. 5–8) are well approximated by Poisson distributions (e.g., Rice 1995), and so the square-root transformation approximately stabilizes and normalizes those variables as well. Thus, a demographic NLAR approximation for a variable N_t is built by transforming the deterministic equation for N_t to the square-root scale, producing the transformed map given by $X_t = h(X_{t-1})$. Adding normal noise for stochasticity produces the NLAR model (Eq. 9). The NLAR model, in conjunction with the square-root transformation, can be regarded as a general method of incorporating demographic stochasticity into a deterministic model. We note that an NLAR process using a logarithmic instead of a square-root transformation is a standard way of incorporating environmental variability (Dennis and Taper 1994, Dennis et al. 1995, Costantino et al. 1997).

The LPA model (Eqs. 1–3) has three state variables, and the demographic NLAR approximation applied to the LPA model produces a multivariate NLAR process. In Eq. 9, X_t becomes a vector of transformed state variables, $h(\cdot)$ becomes a vector-valued function, and E_t becomes a vector of noise variables. Applying the square-root transformation to Eqs. 1–3, and adding noise, yields the following for the stochastic demographic LPA model:

$$\sqrt{L_t} = \sqrt{bA_{t-1}\exp(-c_{el}L_{t-1} - c_{ea}A_{t-1})} + E_{1t} \quad (10)$$

$$\sqrt{P_t} = \sqrt{L_{t-1}(1 - \mu_l)} + E_{2t} \quad (11)$$

$$\sqrt{A_t} = \sqrt{P_{t-1}\exp(-c_{pa}A_{t-1}) + A_{t-1}(1 - \mu_a)} + E_{3t}. \quad (12)$$

The terms $E_t = (E_{1t}, E_{2t}, E_{3t})'$ constitute a random noise vector assumed to have a joint normal probability distribution with a mean vector of zeros and a diagonal variance–covariance matrix denoted by $\mathbf{\Sigma}$. The demographic nature of the stochasticity would stipulate that the noise variables are uncorrelated with each other within a time unit (off-diagonal elements of the matrix $\mathbf{\Sigma}$ are zero) as well as uncorrelated through time. The deterministic skeleton of the model (Eqs. 1–3 transformed) is obtained by setting $\mathbf{\Sigma} = 0$, or equivalently, by letting E_{1t}, E_{2t}, and E_{3t} equal zero.

As written, the demographic NLAR model with normal noise (Eqs. 10–12) can produce negative values for the (transformed) state variables, because the normal noise variables have a nonzero chance of being negative and of large magnitude. Such instances have negligible probabilities under the model parameter values associated with our data. In the rare instances in our simulations when noise produced a negative value of a state variable, the state variable was set to zero. Unlike the situation for the logarithmic transform under environmental variability, zero values for state variables are used in the square-root transform under demographic variability just like any other values and do not require special handling.

For the data from the second transitions experiment (Costantino et al. 1997), we compared the demographic (square-root) and environmental (logarithmic) transformations, as well as a third transformation involving a weighted mixture of demographic and environmental stochasticity. We estimated the parameters of the resulting stochastic LPA models and conducted diagnostic analyses of the residuals (homoscedasticity, autocorrelations, and normality of residuals). Our comparative diagnostic analyses, to be reported in a separate paper, suggested that the model for demographic stochasticity is superior. This is not surprising. The second transitions experiment produced time series with many low (single-digit) values of state variables, due to the experimental manipulations of the treatment populations. Demographic variability is known to be more important for low population sizes (see Simberloff 1988). Therefore, despite the fact that we used environmental noise in our first report (Costantino et al. 1997), the analyses in the present paper are based on the stochastic demographic LPA model given by Eqs. 10–12. However, the qualitative predictions of the fitted models (cycles, chaos, etc.) for both formulations were nearly identical.

The dominant Liapunov exponent

The dominant Liapunov exponent (LE) quantifies the tendency of a deterministic model to be sensitive to initial conditions. It is an index calculated for a trajectory of a deterministic model. At each point of a trajectory there is a maximum rate at which all nearby trajectories can diverge from or converge to one another. The LE is the average of these local maximum rates taken over all points of the trajectory. Thus, in this sense the LE of a trajectory can be thought of as a long-run average rate of exponential divergence or convergence of nearby trajectories. For almost all trajectories converging to an attractor such as a stable point, stable cycle, or strange attractor, the LEs of the trajectories will be identical to the LE of the attractor because the effects of the initial conditions on the averages become washed out. The LE of an attractor is defined as the LE of a dense trajectory on the attractor (that is, a trajectory that comes arbitrarily close to every point on the attractor). A nonchaotic trajectory such as a periodic cycle can exist on a chaotic attractor, but such a trajectory is not dense.

For a bounded trajectory that is not asymptotic to a periodic cycle, a positive LE is an indication of a chaotic attractor (Alligood et al. 1997). If the LE is positive, tiny changes in initial conditions are magnified on average along the trajectory. A negative LE indicates that trajectories differing by tiny changes in initial conditions tend on average to converge; such is the case with a stable point equilibrium or a stable periodic cycle. A stable invariant loop has an LE of zero: on average along a trajectory tiny changes in initial conditions are neither magnified nor diminished.

The LE for the trajectories of the LPA model (Eqs. 1–3) can be computed by iteration. Let $\mathbf{J}_t$ be the Jacobian matrix of the LPA model evaluated at the values L_t, P_t, and A_t, that is,

$$\mathbf{J}_t = \begin{pmatrix} -c_{el}bA_tg_{1t} & 0 & b(1 - c_{ea}A_t)g_{1t} \\ 1 - \mu_l & 0 & 0 \\ 0 & g_{2t} & -c_{pa}P_tg_{2t} + (1 - \mu_a) \end{pmatrix} \quad (13)$$

where, for brevity, $g_{1t} = \exp(-c_{el}L_t - c_{ea}A_t)$ and $g_{2t} = \exp(-c_{pa}A_t)$. Also, let λ_t be defined as a ''geometric mean'' of the norm of the products of the Jacobian matrices:

$$\lambda_t = (1/t)\ln\|\mathbf{J}_t\mathbf{J}_{t-1}\mathbf{J}_{t-2}\cdots\mathbf{J}_2\mathbf{J}_1\|. \quad (14)$$

Here ''$\|\cdot\|$'' denotes any matrix norm (we used the Euclidean norm, $\|\mathbf{M}\| = \sqrt{\Sigma_i \Sigma_j m_{ij}^2}$, where m_{ij} is the element in the ith row and jth column of a matrix $\mathbf{M}$). The LE can in principle be computed as

$$\lambda = \lim_{t\to\infty} \lambda_t \quad (15)$$

for any positive initial condition. This definition is analogous to the eigenvalue for linear stability analysis; here the linearization is ''averaged'' over the long-term trajectory of the population as it visits points on the attractor. If the attractor is a stable point equilibrium, then the LE is identical to the logarithm (of the modulus

of) the largest eigenvalue of $\mathbf{J}_t$ evaluated at the equilibrium (the eigenvalue commonly used in stability analysis of a discrete-time system; May 1974*b*).

The definition of the LE can be extended to the stochastic model (Eqs. 10–12). In this case, the average used to calculate the trajectory LE does not converge to the LE averaged on a deterministic attractor. Rather, the trajectory LE converges to the LE averaged over the stationary probability distribution for the stochastic population (Crutchfield et al. 1982, Kifer 1986, McCaffrey et al. 1992, Ellner and Turchin 1995). However, one must be careful about the interpretation of the ''sensitivity to initial conditions'' implied by a positive stochastic Liapunov exponent (SLE), since stochastic models do not have chaotic attractors and two independent stochastic processes will always drift apart due to the random nature of their dynamics. A positive SLE is an indication that a population spends a large amount of time in a state space region where deterministic trajectories would diverge. Such regions include not only strange attractors but also regions near unstable equilibria and other repellors; in stochastic models, such regions can be revisited often. Thus, the SLE measures something different from the deterministic LE. We develop this point further in the *Discussion,* below.

There are several practical problems with using Eq. 15 directly to compute λ. The matrix product is numerically unstable for large *t,* and, unfortunately, extremely large values of *t* are usually needed for convergence. Care must be taken to minimize the accumulation of numerical roundoff error. Finally, intelligent decisions must be made about the criterion for convergence, especially when *t* is large. In the *Appendix* we describe our algorithm for overcoming these difficulties.

Experimental data

The experiment, described below, was designed explicitly to test the predictions of the deterministic skeleton of the LPA model. Parameter estimates from an earlier experiment (Costantino et al. 1995) predicted a sequence of changes in dynamical behavior from equilibria to invariant loops and periodic cycles to chaos to three cycles as the parameter c_{pa} was increased from 0 to 1 with $\mu_a = 0.96$ (Dennis et al. 1997). In the current study we test that prediction.

We experimentally set the adult mortality rate at $\mu_a = 0.96$ and manipulated the adult recruitment rate so that it would equal $P_t\exp(-c_{pa}A_t)$, with values of c_{pa} set at 0.00, 0.05, 0.10, 0.25, 0.35, 0.50, and 1.00. There was also an unmanipulated control treatment. Twenty-four cultures of the RR strain of the flour beetle *Tribolium castaneum* were initiated with 250 L-stage insects, 5 P-stage animals, and 100 A-stage sexually mature young adults. Three populations were randomly assigned to each of the eight treatments. Each population was maintained in a half-pint (237 mL) milk bottle with 20 g of standard media and kept in a dark incubator at 32°C. Every 2 wk the L-, P-, and A-stages were censused and returned to fresh media, and dead adults were counted and removed. This procedure was continued for 80 wk. Adult mortality was set by removing or adding adults at the time of a census to make the fraction of adults that died during the interval equal to 0.96. Recruitment rates into the adult stage were manipulated by removing or adding young adults at the time of a census to make the number of new adult recruits consistent with the treatment value of c_{pa}. To counter the possibility of genetic changes in life-history characteristics, at every other census the adults returned to the population after the census were obtained from separate stock cultures maintained under standard laboratory conditions. Earlier analyses of this experiment were presented by Costantino et al. (1997) and Desharnais et al. (1997).

Parameter estimation

The method of conditional least squares (CLS) was used for estimation of the parameters in the stochastic demographic LPA model (Eqs. 10–12). CLS methods relax many distributional assumptions about the noise variables in the vector E_t (Klimko and Nelson 1978, Tong 1990). CLS estimates are consistent (converge to the true parameters as sample size increases), even if E_t is non-normal and autocorrelated, provided the stochastic model (Eq. 9) has a stationary distribution.

CLS estimates are based on the sum of squared differences between the value of a variable observed at time *t* and its expected (or one-step forecast) value, given the observed state of the system at time $t - 1$. For fitting the LPA model to a single time series, there are three such conditional sums of squares:

$$Q_1(b, c_{el}, c_{ea}) = \sum_{t=1}^{q}\left(\sqrt{l_t} - \sqrt{ba_{t-1}\exp(-c_{el}l_{t-1} - c_{ea}a_{t-1})}\right)^2 \quad (16)$$

$$Q_2(\mu_l) = \sum_{t=1}^{q}\left(\sqrt{p_t} - \sqrt{l_{t-1}(1 - \mu_l)}\right)^2 \quad (17)$$

$$Q_3(c_{pa}) = \sum_{t=1}^{q}\left(\sqrt{a_t} - \sqrt{p_{t-1}\exp(-c_{pa}a_{t-1}) + a_{t-1}(1 - \mu_a)}\right)^2. \quad (18)$$

Here l_t, p_t, and a_t, $t = 0, 1, \ldots, q$ are the observed census counts for the three life stages. The conditional sums of squares are constructed on the square-root scale because that is the scale on which we assume noise is additive (Eqs. 10–12). Parameter μ_a was estimated directly in the control cultures as a binomial probability from the counts of dead adults and the number of adults at risk of mortality at each census interval.

To estimate c_{pa} in the control cultures, Eq. 18 was used with the value of μ_a fixed at the binomial estimate. Eq. 18 was not used for the treatment cultures, because c_{pa} and μ_a were experimentally fixed in those cultures.

CLS estimates for one population minimize the conditional sums of squares (Eqs. 16–18). Our data (see *Experimental data*, above) consisted of 24 populations: three populations in each of eight treatments, with each population initiated at time $t = 0$ and halted at time $t = 40$. If Q_{ijk} is the conditional sum of squares for state variable i in the jth treatment in the kth population, then the total conditional sum of squares for the ith state variable was calculated as

$$Q_i = \sum_{j=1}^{8} \sum_{k=1}^{3} Q_{ijk}. \tag{19}$$

Thus, just one set of CLS parameter estimates was obtained for the whole experiment. Three separate numerical minimizations are required, one for each Q_i. We found the Nelder-Mead simplex algorithm (Press et al. 1992) convenient. Alternatively, the CLS estimates can be obtained by minimizing Q_1, Q_2, and Q_3 with a standard nonlinear regression package.

The noise variances (diagonal elements in the variance-covariance matrix $\mathbf{\Sigma}$ of E_t, Eqs. 10–12) were estimated using the conditional residuals (Dennis et al. 1995). We estimated noise covariances as well, to check the assumption under demographic variability that the random departures from the model skeleton are uncorrelated (that is, the off-diagonal elements of $\mathbf{\Sigma}$ are 0). Let $\mathbf{x}_t$ denote the vector $[\sqrt{l_t}, \sqrt{p_t}, \sqrt{a_t}]'$ of observed, transformed stage abundances in a population at time t. Thus, $\mathbf{x}_0$, $\mathbf{x}_1$, $\mathbf{x}_2$, . . . is a time series of vector observations arising from one of the experimental populations. Also, let $\hat{\mathbf{h}}(\mathbf{x}_{t-1})$ denote the vector of functions in the model skeleton (Eq. 9) evaluated at $\mathbf{x}_{t-1}$ using the CLS parameter estimates. Each population in the experiment yielded a series of residual vectors defined as

$$\hat{\mathbf{e}}_t = \mathbf{x}_t - \hat{\mathbf{h}}(\mathbf{x}_{t-1}) \tag{20}$$

for $t = 1, 2, \ldots, 40$. The noise variances and covariances for the three control populations were estimated from the sum of squares and crossproducts matrix calculated with the 120 residual vectors. A separate variance–covariance matrix was estimated for the 21 treatment populations, to allow for the possibility that the adult manipulations might alter the stochastic variability in the L and P stages, particularly the variability in L-stage recruitment. The control residual vectors were 3×1; however, the treatment residual vectors were 2×1 (L and P stages only) because the experimental manipulations rendered the adult populations deterministic.

The LE and SLE corresponding to each experimental treatment are functions of LPA model parameters. Point estimates of the LE for each treatment were obtained from the deterministic model (Eqs. 1–3) evaluated at the CLS parameter estimates of b, c_{el}, c_{ea}, and μ_l, and relevant CLS (control) or fixed (treatment) values of c_{pa} and μ_a. Point estimates of the SLE for each treatment were calculated with the stochastic model (Eqs. 10–12), using the CLS estimates of b, c_{el}, c_{ea}, and μ_l, relevant values of c_{pa} and μ_a, and the estimates of the noise variances obtained from the residuals of the fitted model.

We also calculated maximum-likelihood (ML) estimates for the LPA parameters in the Poisson-binomial model (Eqs. 4–8). The purpose was to compare the CLS estimates from the NLAR approximation (Eqs. 10–12) with the ML estimates. With the Poisson-binomial model, the likelihood function for each state variable is a product of one-step Poisson or binomial probabilities. For illustration, we focus on the time series emerging from one population. The likelihood function for the parameters in the L-stage model is

$$L_1(b, c_{el}, c_{ea}) = \prod_{t=1}^{q} \exp[ba_{t-1}\exp(-c_{el}l_{t-1} - c_{ea}a_{t-1})] \times [ba_{t-1}\exp(-c_{el}l_{t-1} - c_{ea}a_{t-1})]^{l_t}/(l_t!). \tag{21}$$

This is a product of Poisson probabilities for the values $l_t (t = 1\ 2, \ldots, q)$, with means as indicated by Eq. 4. The likelihood functions for the parameters in the models for the other state variables are products of binomial probabilities:

$$L_2(\mu_l) = \prod_{t=1}^{q} \binom{l_{t-1}}{p_t} (1 - \mu_l)^{p_t} (\mu_l)^{l_{t-1}-p_t} \tag{22}$$

$$L_3(c_{pa}) = \prod_{t=1}^{q} \binom{p_{t-1}}{r_t} [\exp(-c_{pa}a_{t-1})]^{r_t} \times [1 - \exp(-c_{pa}a_{t-1})]^{p_{t-1}-r_t} \tag{23}$$

$$L_4(\mu_a) = \prod_{t=1}^{q} \binom{a_{t-1}}{s_t} (1 - \mu_a)^{s_t} (\mu_a)^{a_{t-1}-s_t}. \tag{24}$$

Here s_t is the number of adults surviving from time $t - 1$ (a_{t-1} minus the number of dead adults counted at time t), and $r_t = a_t - s_t$. The ML estimates are the values of the unknown parameters c_{el}, c_{ea}, μ_l, and in the control cultures c_{pa} and μ_a, that jointly maximize the likelihood functions. As with the CLS estimates, all the time series from the experiment were combined to obtain one set of ML parameter estimates. The actual likelihood functions used were products of functions like Eqs. 21–24 taken over all the experimental populations. The ML estimates were calculated by numerical maximization (Eqs. 22 and 24 also admit simple closed-form solutions for the ML estimates).

Model evaluation

In two previous studies we withheld at least half of the data from the parameter estimation process and

used the withheld data in model prediction/validation analyses (Dennis et al. 1995, 1997). In the present study we used all the data in estimation in order to concentrate all the available information into confidence statements about dynamics. The analyses described here are therefore to be interpreted as goodness-of-fit analyses. Nonetheless, because the model has so few parameters, the data are so abundant, the experimental manipulations are so distinct, and the model-predicted responses to those manipulations are so sharp, evidence that the LPA model fits this experiment serves as a fairly severe test of the model.

Our main criterion for evaluating goodness-of-fit was R^2. We calculated a generalized R^2 statistic to quantify the overall influence of the LPA model skeleton. For state variable i in the jth experimental treatment, the conditional sum of squares $\hat{Q}_{ij}$ was calculated by using the CLS parameter estimates in Eq. 16, 17, or 18. A second conditional sum of squares, $\hat{S}_{ij}$, was calculated using the sample mean of the (square-root transformed) state variable values as the one-step predicted value. For example, for the L-stage, using subscripts to denote the kth population in the jth treatment,

$$\hat{S}_{1j} = \sum_{k=1}^{3} \sum_{t=1}^{40} \left(\sqrt{l_{jkt}} - m_{1j}\right)^2 \tag{25}$$

where

$$m_{1j} = \frac{1}{120} \sum_{k=1}^{3} \sum_{t=1}^{40} \sqrt{l_{jkt}} \tag{26}$$

is the sample mean of the square-root transformed L-stage abundances in the jth treatment. The generalized R^2 value for state variable i in the jth treatment was then defined as

$$R^2_{ij} = 1 - (\hat{Q}_{ij}/\hat{S}_{ij}). \tag{27}$$

An overall R^2 was calculated for the ith state variable as

$$R^2_i = 1 - \left[\left(\sum_{j=1}^{8} \hat{Q}_{ij}\right) \Big/ \left(\sum_{j=1}^{8} \hat{S}_{ij}\right)\right]. \tag{28}$$

It will be noted that each treatment retains its own mean in the overall R^2 formula, rather than pooling observations across treatments to calculate a common mean.

The model was further evaluated using residual analyses. If the skeleton captures the essential dynamical behavior, the leftover variability on some appropriate scale should be just noise. Additionally, the demographic scale we selected for the noise (as reflected through Eqs. 10–12) should turn out to be an appropriate one. In order to examine these assumptions, the residuals for each stage in each culture (Eq. 20) were subjected to the following diagnostic procedures. First, the first-order and second-order autocorrelations of the residuals were calculated. Autocorrelation of residuals indicates a relationship between successive prediction errors, and thus might suggest a systematic lack of fit between model and data. Second, the residuals were screened in standard diagnostic plots, including normal quantile–quantile plots, and tested for lack of fit to a normal distribution using the Lin-Mudholkar statistic (see Tong 1990). The Lin-Mudholkar statistic was designed for power against asymmetrical alternatives (Lin and Mudholkar 1980). Asymmetry is a main feature that is visually detectable in normal quantile–quantile plots; we report the Lin-Mudholkar statistic in this paper to condense the information from many figures. While CLS estimates are robust to autocorrelation and departure from normality, the diagnostic screening helps determine whether the demographic noise model adequately portrays the stochastic variability in the system.

Bootstrap confidence intervals

If the experiment could somehow be repeated, how much variability in the results might be expected? If the fitted LPA model is chaotic for a particular treatment, would it reliably be chaotic again? We deemed it crucial to obtain an estimate of how variable the estimated dynamic behaviors might be under stochastic repetitions of the experiment. This variability is sometimes termed ''sampling variability,'' though it must be kept in mind that what is ''sampled'' here are realizations of the stochastic population process.

We used a bootstrapping technique for time-series models. A version of the technique was used by Falck et al. (1995*a*, *b*); we incorporated a centering modification, described below, that was recommended in the statistics literature.

Recall that the residual vectors (Eq. 20) from the 24 populations were in two groups, control and treatment. For each group of residual vectors, the sample mean vector was calculated, and the resulting vector was subtracted from each residual in the group. These centered residuals were used in our bootstrapping procedure. The centering is theoretically important because the collection of centered residual vectors provides a statistically consistent estimate of the (possibly multivariate) noise distribution (Leger et al. 1992). In our data, the sample means of the residuals were near 0, and the centering was of little consequence.

To construct a bootstrapped time series for a single population, 40 residual vectors were sampled with replacement from the appropriate group (control or treatment) of centered residuals. The bootstrapped time series was started at the actual initial value $\mathbf{x}^*_0 = \mathbf{x}_0$, and was constructed with the relationship

$$\mathbf{x}^*_t = \hat{\mathbf{h}}(\mathbf{x}^*_{t-1}) + \hat{\mathbf{e}}^*_t \tag{29}$$

where $\hat{\mathbf{e}}^*_t$ is the tth sampled residual vector, $\hat{\mathbf{h}}(\mathbf{x}^*_{t-1})$ is the vector of functions in the model skeleton (Eq. 9) evaluated using the CLS parameter estimates and relevant values of c_{pa} and μ_a. The resulting time series of vectors, $\mathbf{x}^*_0, \mathbf{x}^*_1, \mathbf{x}^*_2, \ldots, \mathbf{x}^*_{40}$, is a kind of simulated trajectory of life stages (square-root scale) for a popu-

lation in a given treatment under the estimated model. In this way, an entire bootstrapped data set of 24 populations in the form of the original data was constructed. The model was then refitted to the bootstrapped data set, yielding a set of bootstrapped CLS parameter estimates.

The process of generating a bootstrapped experiment (using the original CLS estimates) and calculating bootstrapped CLS estimates was repeated 2000 times, yielding 2000 sets of bootstrapped CLS parameter estimates. This collection forms a statistically consistent estimate of the multivariate sampling distribution of the CLS parameter estimates. The collection thus provides confidence intervals for parameters, or functions of parameters such as LEs. For each LPA model parameter, we used the 2.5th and 97.5th sample percentiles of the bootstrapped estimates as a 95% confidence interval.

Additionally, the collection provides estimates of how much variability there is in the types of dynamic behaviors estimated for each treatment. For each of the 2000 bootstrapped parameter sets, the dynamic properties of the corresponding LPA model were ascertained. First, the LEs and SLEs for each treatment were calculated with each bootstrapped parameter set. Second, if the LE was negative, the period of the attractor for the LPA skeleton was determined. The result for each treatment was a frequency count of different dynamic behaviors. At a given treatment, the proportion of the bootstrapped parameter sets that yielded, for instance, a two-cycle (i.e., a two-period cycle) is a valid estimate of the probability that a parameter set drawn from the CLS sampling distribution would produce a two-cycle.

TABLE 1. Conditional least squares (CLS) and maximum-likelihood (ML) estimates of the LPA model parameters and their 95% bootstrapped confidence intervals.

Parameter†	CLS estimate	ML estimate	95% confidence interval
b	10.45	10.67	(10.04, 10.77)
μ_l	0.2000	0.1955	(0.1931, 0.2068)
μ_a†	0.007629	0.007629	(0.006769, 0.008489)
c_{el}	0.01731	0.01647	(0.01611, 0.01759)
c_{ea}	0.01310	0.01313	(0.01285, 0.01340)
c_{pa}‡	0.004619	0.004135	(0.004446, 0.004792)

† Definitions: b = number of larval recruits per adult per unit time in the absence of cannibalism; μ_l = probability of larval mortality in one unit time; μ_a = probability of adult mortality in one unit time; c_{el} = larva–egg cannibalism coefficient; c_{ea} = adult–egg cannibalism coefficient; c_{pa} = adult–pupa cannibalism coefficient.

‡ Control cultures only. Estimate and confidence interval for μ_a was obtained directly from counts of dead adults. The CLS estimates of the variances and covariances of the random elements (matrix $\hat{\mathbf{\Sigma}}$) are: $\hat{\sigma}_{11} = 1.621$, $\hat{\sigma}_{12} = -0.1336$, $\hat{\sigma}_{13} = -0.01339$, $\hat{\sigma}_{22} = 0.7375$, $\hat{\sigma}_{23} = -0.0009612$, and $\hat{\sigma}_{33} = 0.01212$ for the controls; and $\hat{\sigma}_{11} = 2.332$, $\hat{\sigma}_{12} = 0.007097$, $\hat{\sigma}_{22} = 0.2374$, and $\hat{\sigma}_{13} = \hat{\sigma}_{23} = \hat{\sigma}_{33} = 0$ for the treatments, where adult mortality and recruitment was manipulated.

RESULTS

Parameter estimates

The CLS (conditional least squares) estimates and 95% bootstrapped confidence intervals for the parameters in the stochastic LPA model (Eqs. 10–12) are given in Table 1. Since μ_a, the adult mortality probability, and c_{pa}, the adult-pupa cannibalism coefficient, were fixed in the manipulated treatments, the point estimates and confidence intervals for these two parameters were obtained from the data on the controls. The confidence intervals indicate that the parameters are estimated with good precision; the half-widths of the confidence intervals ranged from around 2% to 11% of the CLS point estimates (Table 1). Also listed in Table 1 are the ML (maximum-likelihood) parameter estimates obtained from the Poisson/binomial model (Eqs. 4–8). The ML estimates were close to the CLS point estimates (Table 1). The ML estimates of b, μ_l, c_{el}, and c_{ea} were well within the 95% CLS confidence intervals. The least similar ML estimate, that of c_{pa} in the control cultures, differed from the CLS estimate by only 10.5%. The binomial ML estimate for μ_a in the control cultures was taken as fixed in the CLS estimation routines, and so is identical in both columns. Overall, the close similarity of the CLS and ML estimates suggests that the NLAR (nonlinear autoregressive) model (Eqs. 10–12) provides a good approximation to the Poisson/binomial model (Eqs. 4–8).

There was little or no correlation between the noise fluctuations of the state variables. The estimated covariances (Table 1) translate into the following correlations: $\hat{\rho}_{12} = -0.10$, $\hat{\rho}_{13} = -0.096$, and $\hat{\rho}_{23} = -0.010$ for the unmanipulated controls, and $\hat{\rho}_{12} = -0.0030$ for the manipulated treatments; despite the large sample sizes, none of these correlations are statistically different from 0. If the fluctuations were environmental in origin, we might expect that the departures of model and data would be related among the life stages (a good time interval for the L stage, say, would be related to whether or not the interval was good for the other stages). The lack of such correlation suggests that the noise is mostly demographic in nature.

The bootstrapped parameter sets provide additional information on the distributional properties of the parameter estimates. The quantile–quantile plots of Fig. 1 compare the observed quantiles of the standardized bootstrapped parameters to those of the standard normal distribution. The lack of departure from straight lines indicates that the estimates are well described with normal probability distributions. In Fig. 2 we show a scatterplot matrix of the bootstrapped parameter vectors. The histograms along the diagonal of the matrix also support the hypothesis that the parameter estimates are normally distributed. The lack of any strong correlations among the parameters, as indicated by the scatterplots, suggests that the model is not overparameterized. These results taken together suggest that the data provided good information about the model parameters.

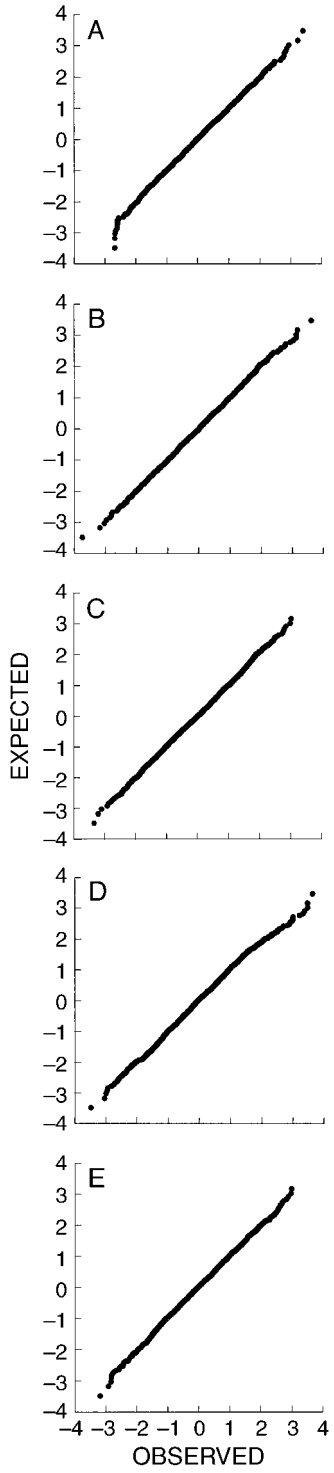

FIG. 1. Normal quantile–quantile plots of the (standardized) bootstrap parameter estimates. Units on both axes are standard deviations. A–E portray results for b, μ_l, c_{el}, c_{ea}, and c_{pa}, respectively. See Table 1 for definitions of parameters.

Estimated dynamics

The deterministic skeleton of the model (Eqs. 1–3), evaluated with the CLS point estimates, forecasts striking changes in dynamical behavior—from point equilibria, to cycles, to chaos—under our experimental conditions. Recall that manipulation of the adult mortality rate and adult recruitment rate provided the means of experimentally controlling the values of the parameters μ_a and c_{pa}. The estimated LPA skeleton yielded an estimate of dynamical behavior at each treatment value of c_{pa} as well as an estimate of the LE (Table 2). A bifurcation diagram was computed with the CLS estimates to show how the estimated attractor changes as the parameter c_{pa} changes (Fig. 3A). Fig. 3A and Table 2 together show the distinctive sequence of transitions in the estimated attractor of the model skeleton that occurs as the value of c_{pa} is varied. The estimated bifurcation diagram (Fig. 3A) closely resembles the one reported earlier for this experiment using environmental noise (Costantino et al. 1997: Fig. 1); in fact, all the parameter estimates except for $\hat{b}$ from the environmental-noise analysis lie within the confidence intervals reported here in Table 1.

For the control cultures, the estimated attractor is a stable point equilibrium (Table 2). For the $c_{pa} = 0.00$ treatment, the estimated behavior is aperiodic cycling on an invariant loop, which has an LE (Liapunov exponent) of 0 (Table 2, Fig. 3A). The loop actually consists of two tiny separate loops in phase space, with deterministic trajectories visiting each tiny loop in alternating time steps, and the result is that the trajectories resemble 2-period cycles. The estimated attractors for the $c_{pa} = 0.05$ and $c_{pa} = 0.35$ treatments are chaotic; the corresponding estimated LEs are positive, and the attractors are ''strange.'' The $c_{pa} = 0.10$ and $c_{pa} = 0.25$ treatments are stable long-period cycles that seem to occur in period-locked ''windows'' among more complex regions of the bifurcation diagram. The corresponding LEs are negative. The graph of the estimated LE as a function of c_{pa} (Fig. 3B) shows great variability in the LE for values of c_{pa} below 0.48 (approximately). The $c_{pa} = 0.50$ treatment produces a stable 3-period cycle, while the $c_{pa} = 1.00$ treatment gives a stable 6-period cycle. However the 6-cycle occurs just after a period-doubling bifurcation of the 3-cycle, and the 6-cycle trajectories resemble a 3-cycle in appearance. The LE estimates for $c_{pa} = 0.50$ and $c_{pa} = 1.00$ are negative.

The estimated SLEs (stochastic Liapunov exponents) differed substantially from the LEs (Table 2). Only the control and the $c_{pa} = 1.00$ treatments had negative SLEs; all the rest of the treatments had positive SLEs. The graph of the estimated SLE value as a function of c_{pa} (Fig. 3C) is positive over a large interval of c_{pa} values below 0.57 (approximately); by contrast the graph of the estimated LE values is jagged, irregular,

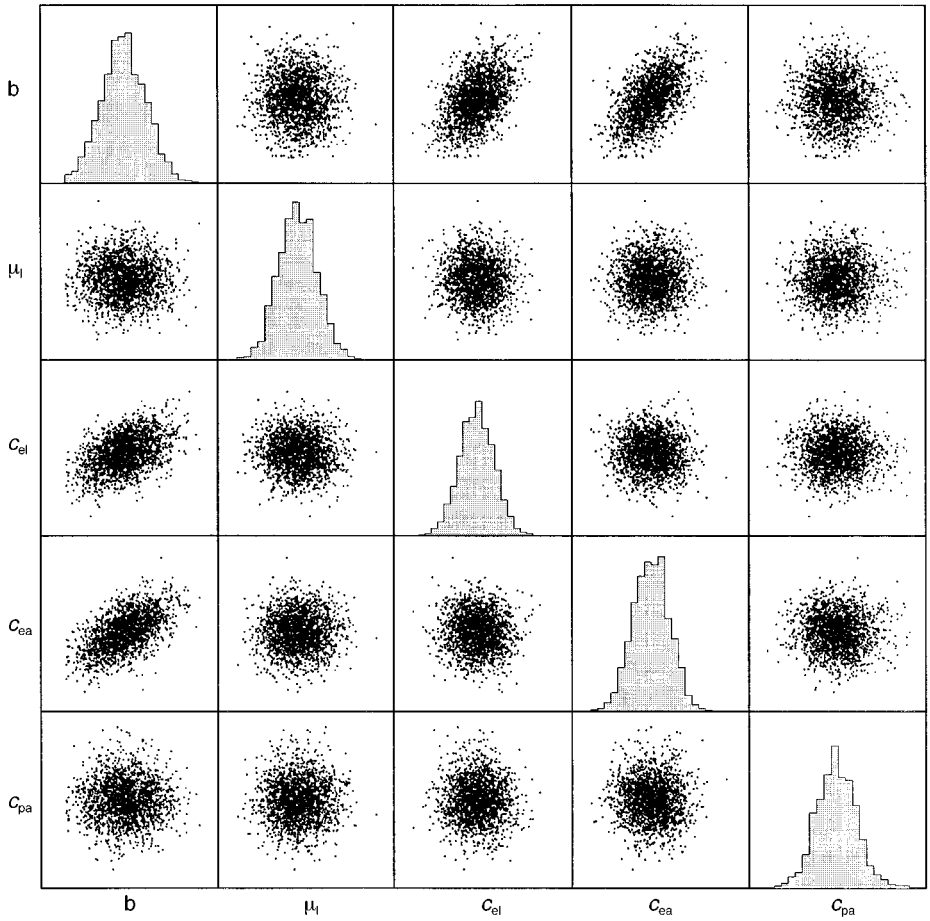

FIG. 2. Scatterplot matrix of the bootstrap parameter estimates. See Table 1 for definitions of parameters.

and has negative as well as positive portions in that region (Fig. 3B).

The bootstrapped parameter estimates allow us to gain an idea of how variable are the estimates of dynamic behavior. The claim, for instance, that the attractor for $c_{pa} = 0.10$ is a 26-cycle (Table 2) is merely a ''point estimate,'' that is, the claim relies on a point estimate of the model parameters. In fact, the 26-cycle is a narrow region of a complex bifurcation diagram (Fig. 3A), and the bifurcation diagram itself changes when model parameters change. If the point estimates were changed to other values within their confidence intervals (Table 2), the behavior of the skeleton at $c_{pa} = 0.10$ might be, say, a cycle with some other period.

Each of the 2000 bootstrapped parameter vectors provided an estimated LE, an estimated SLE, and an estimate of the dynamical behavior of the skeleton attractor for every treatment. The 2.5 and 97.5 percentiles of the 2000 bootstrapped LE and SLE values at each treatment were used to form 95% confidence intervals for the LE and SLE of that treatment (Table 2). The control and $c_{pa} = 0.10$, 0.25, 0.50, and 1.00 treatments,

TABLE 2. Deterministic attractors and estimates (and 95% bootstrapped confidence intervals) of deterministic and stochastic Liapunov exponents (LE).

Treatment†	Attractor	Deterministic LE	Stochastic LE
Control	equilibrium	−0.046 (−0.047, −0.045)	−0.044 (−0.045, −0.044)
$c_{pa} = 0.00$	invariant loop	0.000 (−0.036, 0.000)	0.009 (−0.007, 0.014)
$c_{pa} = 0.05$	chaotic	0.029 (−0.227, 0.029)	0.045 (−0.042, 0.046)
$c_{pa} = 0.10$	26-cycle	−0.109 (−0.115, −0.0004)	0.060 (0.056, 0.062)
$c_{pa} = 0.25$	8-cycle	−0.076 (−0.090, −0.071)	0.068 (0.066, 0.071)
$c_{pa} = 0.35$	chaotic	0.096 (−0.066, 0.100)	0.053 (0.049, 0.055)
$c_{pa} = 0.50$	3-cycle	−0.089 (−0.101, −0.080)	0.019 (0.013, 0.025)
$c_{pa} = 1.00$	6-cycle	−0.003 (−0.025, −0.0003)	−0.075 (−0.087, −0.063)

† The adult–pupa cannibalism coefficient is represented as c_{pa}.

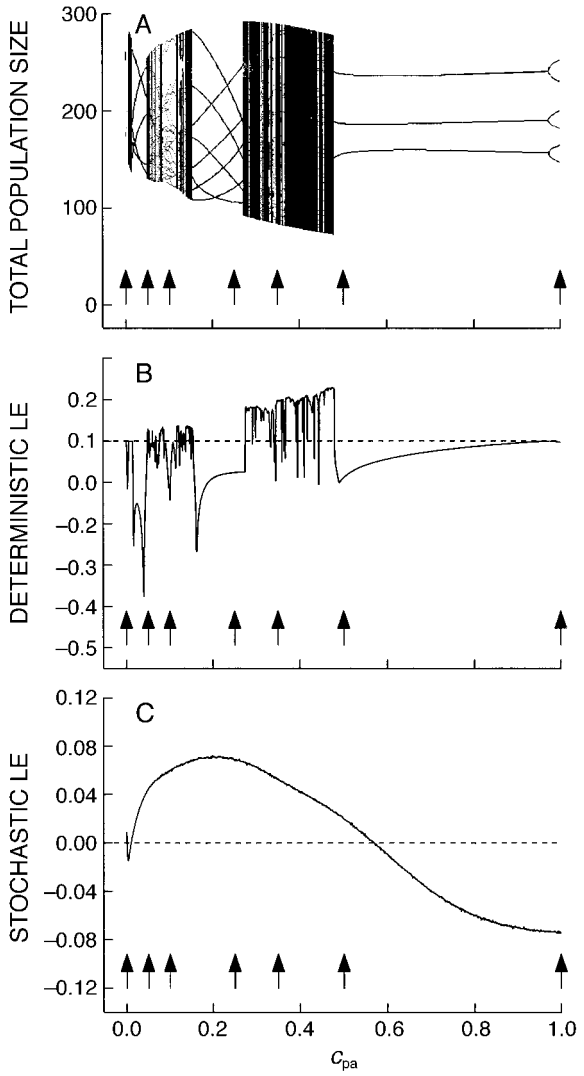

FIG. 3. Transitions in predicted deterministic dynamics for the point estimates of the parameters as reflected by (A) the bifurcation diagram for total population size (L-stage + P-stage + A-stage [see Table 3 for definitions of stages]), (B) deterministic Liapunov exponents (LE), and (C) stochastic Liapunov exponents, for c_{pa} values (adult–pupa cannibalism coefficients) ranging from 0 to 1. Arrows indicate experimentally fixed values of c_{pa}.

had LE confidence intervals over values that were strictly negative. However, for $c_{pa} = 0.10$, most of the bootstrappped parameter vectors predicted high-period cycles with weak stability and LEs negative but near 0; the 97.5 percentile was just below 0 (Table 2). Similarly, for $c_{pa} = 1.00$, the 97.5 percentile was negative but close to 0. The $c_{pa} = 0.00$ treatment had an LE confidence interval with 0 included as the upper bound. This reflects an area of parameter space in which most parameter vectors yield stable cycles (LE < 0), but a measurable proportion of vectors result in invariant loops (LE $= 0$).

The LE confidence intervals for the $c_{pa} = 0.05$ and $c_{pa} = 0.35$ treatments include positive values. The LE confidence interval for the $c_{pa} = 0.35$ treatment, in fact, lies mostly in the positive range, with just a small portion overlapping into negative values. Later in this paper (see *Bootstrapped attractors,* below) we show that the negative values correspond mostly to high-period cycles of unusual periods (e.g., 19-cycles). Thus, we confidently claim that the attractor for the $c_{pa} = 0.35$ treatment is either chaotic or nearly aperiodic in relation to the length of our time series (40 time steps). The $c_{pa} = 0.05$ treatment is odd in that the LE point estimate is on the upper edge (to two decimal places) of the confidence interval. We show below (see *Bootstrapped Liapunov exponents*) how this stems from extreme skewness of the sampling distribution of LE estimates for the $c_{pa} = 0.05$ treatment.

The confidence intervals for the SLEs were more straightforward. Two of the treatments, the control and the $c_{pa} = 1.00$ treatments, had SLE confidence intervals that were strictly negative. Five of the treatments, $c_{pa} = 0.05$, 0.10, 0.25, 0.35, and 0.50, had SLE confidence intervals over strictly positive values. The $c_{pa} = 0.00$ treatment had an SLE confidence interval that included positive and negative portions. While one can debate about whatever property it is that SLE measures, estimating the SLE appears more stable than estimating the LE. We show below (see *Bootstrapped Liapunov exponents*) that the sampling distributions of the SLE estimates for all the treatments are fairly well behaved.

Bootstrapped bifurcation diagrams

The variability of the estimates of attractor behavior and deterministic LEs can be better understood by graphically exploring parameter space. The joint confidence intervals for the parameters can be regarded as a (hyper)rectangular region of parameter space, within which any parameter vector is plausible under the experimental evidence. (While the region is not strictly a *joint* 95% confidence region, the parameter estimates are nearly independent (see Fig. 2), and so the region forms an approximate (conservative) 95% confidence region.) The region generously indicates how much variability might be expected under repeated sampling. A fascinating picture of the variability in the estimates of the skeleton attractor resulted from plotting the c_{pa} bifurcation diagram for different parameter vectors in the region.

In Fig. 4 the c_{pa} bifurcation diagram is plotted for nine combinations of b and c_{el} values, with the other parameters held fixed at the CLS estimates. The three rows represent respectively the upper 95% confidence limit, the CLS estimate, and the lower 95% confidence limit, of the parameter b. The columns represent the same limits for the parameter c_{el}. The center diagram of Fig. 4 is, for reference, the CLS point estimate of the bifurcation diagram (as in Fig. 3). There is a strong qualitative similarity in the nine diagrams. For values of c_{pa} less than $\sim$0.5 the diagrams show a region of complex behavior, with a large window of periodic

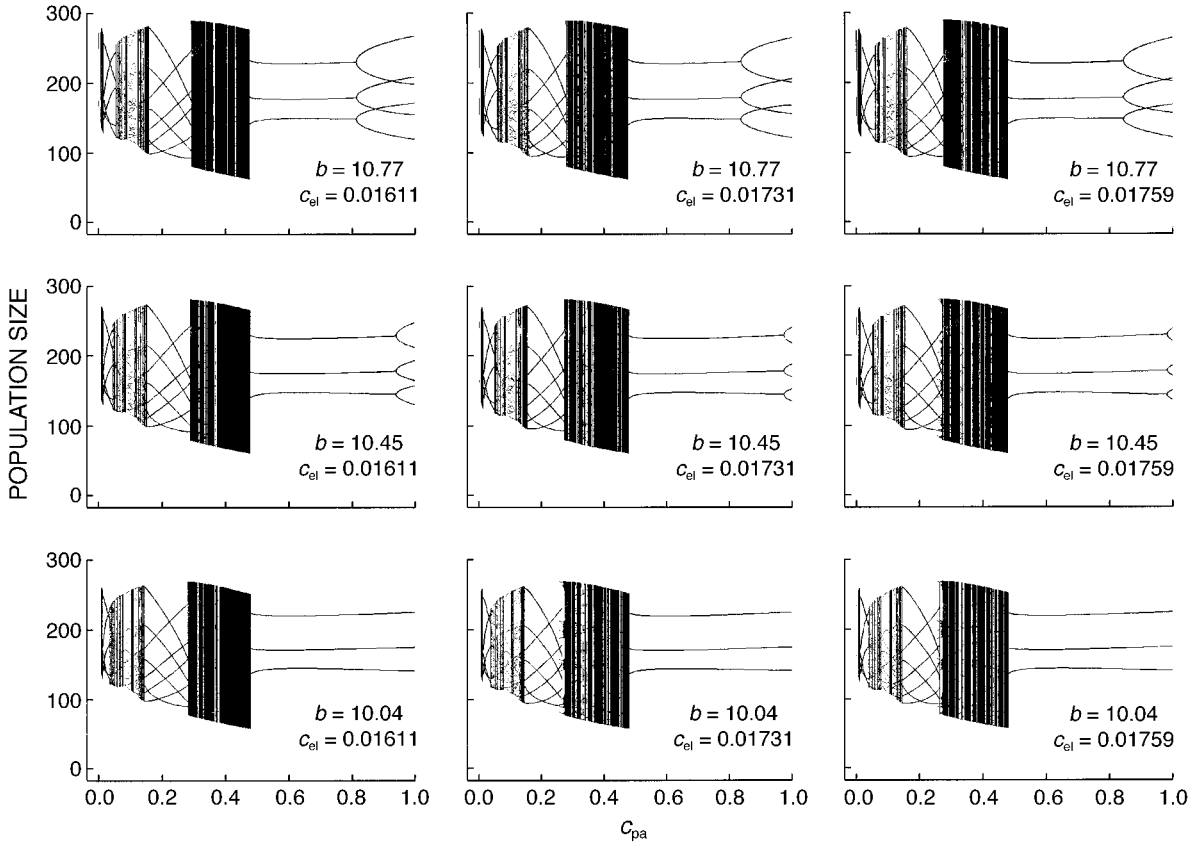

FIG. 4. Bifurcation diagrams for total population size (L-stage + P-stage + A-stage) plotted for all the combinations of the upper and lower 95% confidence limits of parameters b (the number of larval recruits per adult per unit time in the absence of cannibalism) and c_{el} (larva–egg cannibalism coefficient) for c_{pa} values (adult–pupa cannibalism coefficients) ranging from 0 to 1.

behavior centered at approximately $c_{pa} = 0.2$. At a value of c_{pa} just under 0.5, the complex behavior gives way abruptly to an extended region of stable 3-cycles. At particular values of c_{pa}, though, there is considerable local variation in the diagrams. For instance, at $c_{pa} = 1.00$, one of our treatment values, the lower row of diagrams (lower value of b) indicates that the attractor is estimated to be a 3-cycle, while in the upper two rows (increasing values of b), the estimated attractor has locally bifurcated into a 6-cycle. Similarly, around the treatment values of $c_{pa} = 0.05$ and 0.10 the bifurcation diagram is locally wispy; the dynamics of the attractors vary between cycles and chaos in intricate lacelike patterns.

The $c_{pa} = 0.35$ treatment lies within the dark, complex behavior region in all nine bifurcation diagrams (Fig. 4). The strange complexities of the attractors are revealed by zooming in for a close-up view. In Fig. 5 the interval from $c_{pa} = 0.34$ to 0.36 in the nine bifurcation diagrams is magnified. Between dark areas of aperiodic chaotic behavior, thin windows appear in which stable, high-period cycles undergo period-doubling bifurcations. Note the considerable variation in the locations of the windows. Similar features would be revealed, fractal-like, upon further magnification. By changing a parameter value a small amount in such regions, the behavior of the attractor can change considerably, from stable cycles to chaos, or the reverse. The parameter values giving rise to periodic behavior (LE < 0) in such regions are sets of positive measure (they have positive volume in parameter space), as are the parameter values giving rise to chaotic attractors (LE > 0).

Bootstrapped Liapunov exponents

Histograms of the bootstrapped LE values show how variability in parameter estimates becomes propagated into the LE estimates (Fig. 6). The bootstrapped LE values for the control treatment form a conventional bell-shaped histogram. The LE values represent estimated local stability strengths of the stable point equilibrium of the skeleton. The LE histograms for the $c_{pa} = 0.25$ and 0.5 treatments are also reasonably bell shaped. The LE values for these treatments represent the estimated local stability strengths of the cyclic attractors. The $c_{pa} = 0.25$ histogram actually extends into the region of positive LE values; 6 out of 2000 bootstrapped LEs were positive (not visible in the resolution of Fig. 6). The LE histograms for the other treatments

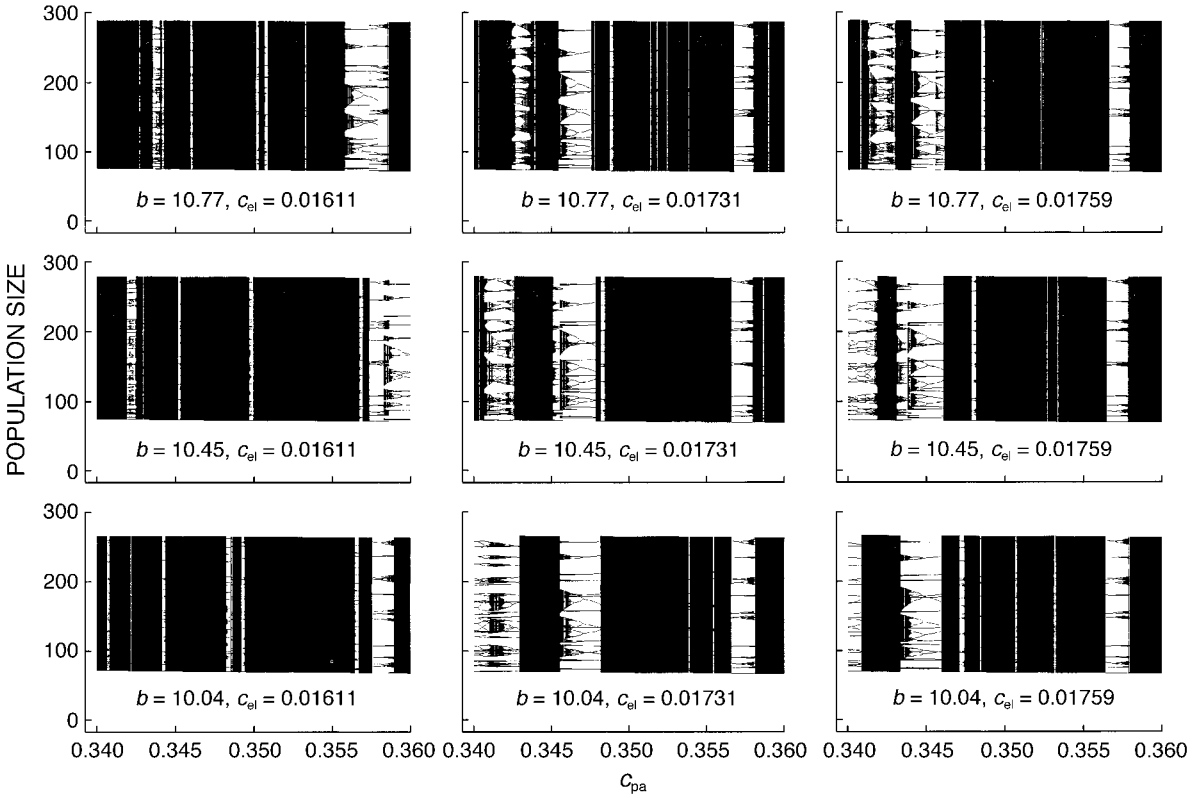

FIG. 5. Bifurcation diagrams plotted for all the combinations of the upper and lower 95% confidence limits of parameters b and c_{el} for c_{pa} values ranging from 0.34 to 0.36 (i.e., a close-up view of a portion of Fig. 4).

are highly skewed and peculiar (Fig. 6). For the c_{pa} = 0.00 treatment, most of the bootstrapped LE values are negative, but there is a spike of frequency at 0. The sampling distribution of the LE estimates here is apparently a mixed discrete and continuous distribution, with the positive probability at 0 giving the proportion of times the dynamic behavior is estimated to be aperiodic cycling on an invariant loop. The c_{pa} = 0.10 treatment has a left-skewed, ramp-shaped histogram of LE values in the negative region, with a visible little tail extending into the positive region (38 out of 2000 bootstrapped LEs were positive). The c_{pa} = 1.00 treatment has a left-skewed, J-shaped histogram of LE values. The LE values for c_{pa} = 1.00 were all strictly negative, though the histogram peak is near 0: the estimated cycles are weakly stable.

Though the LE histograms for the c_{pa} = 0.05 and 0.35 treatments have negative portions, they extend considerably into the positive region (Fig. 6). For the c_{pa} = 0.05 treatment, the skeleton attractor is highly variable in this region of parameter space (recall Fig. 4). A variety of stable cycles (1218 out of 2000), as well as chaos (782 out of 2000), are plausible behaviors estimated for the attractor, according to the bootstrapped LE values for c_{pa} = 0.05 (Fig. 6). The bulk (1670 out of 2000) of the bootstrapped LE values for the c_{pa} = 0.35 treatment are positive (Fig. 6). The remaining negative portion of the LE values for that treatment correspond to small windows of high-period stable cycles in an otherwise complex bifurcation diagram (recall Fig. 5).

The histograms for the bootstrapped SLE values were bell shaped for all the treatments (Fig. 7). The control and c_{pa} = 1.00 treatments had SLE histograms that were unambiguously within the negative region. The c_{pa} = 0.05, 0.10, 0.25, 0.35, and 0.5 treatments had SLE histograms that were unambiguously positive. The c_{pa} = 0.00 treatment had an SLE histogram that straddled 0. The normal-like shape of the histograms suggests that the SLE is a stable function of the model parameters for which the conventional asymptotic normality theory of maximum-likelihood estimates might apply (e.g., Lehmann 1983). We remark that the calculation of the bootstrapped SLEs for these histograms with appropriate numerical precision and safeguards (see *Appendix*) required weeks of running time on a contemporary Pentium computer.

Bootstrapped attractors

The 2000 bootstrapped parameter sets provided, for each treatment, 2000 estimated attractors. We summarized the frequencies of different dynamical behaviors of those attractors in a series of pie diagrams (Fig. 8). The control and c_{pa} = 0.50 treatments each showed

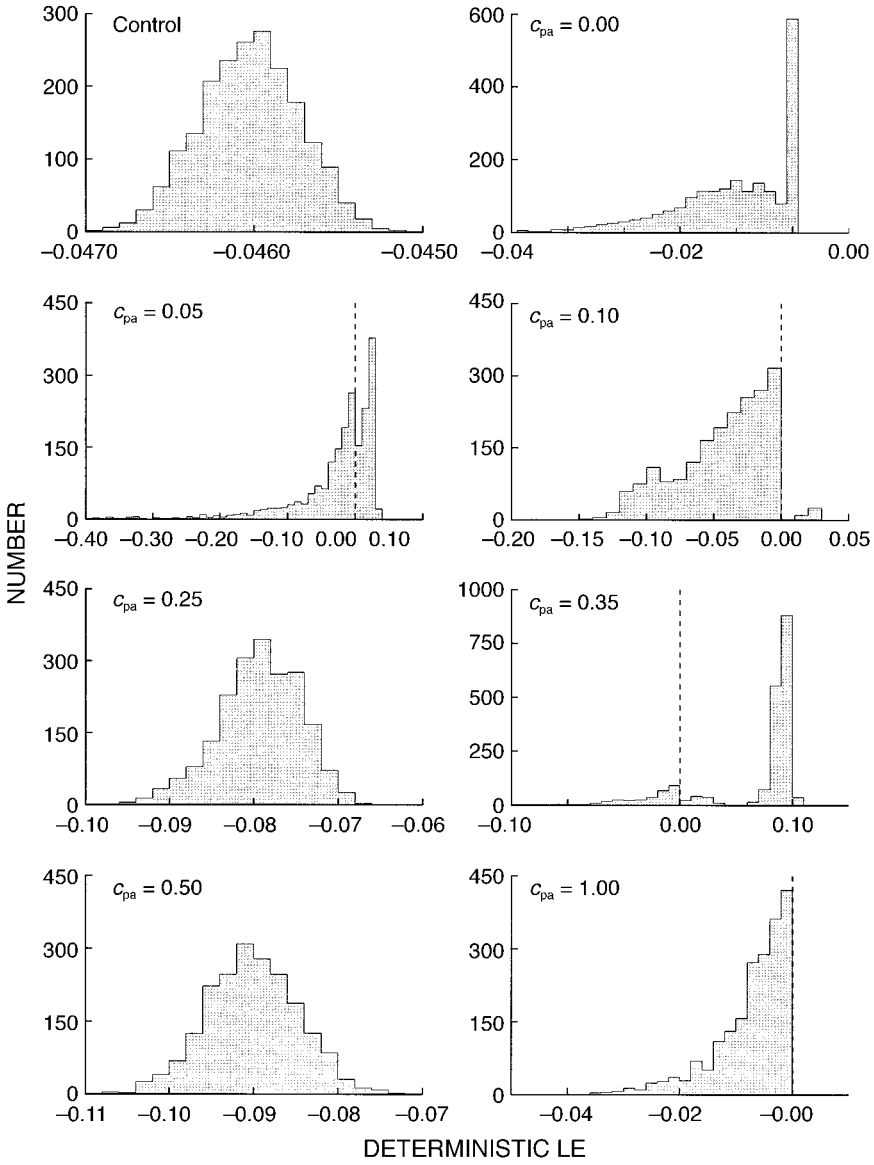

FIG. 6. Histograms of the 2000 bootstrap estimates of the deterministic Liapunov exponents (LE) for each experimental treatment. Not visible on the c_{pa} = 0.25 histogram are six positive LEs.

entirely one type of behavior: stable point equilibrium for the control, and stable 3-cycles for the c_{pa} = 0.50 treatment. The c_{pa} = 0.25 treatment displayed stable 8-cycles nearly entirely, with a tiny portion (0.3%) of the attractors being chaotic. These three treatments had ordinary bell-shaped histograms of bootstrapped LE values (recall Fig. 6). The c_{pa} = 1.00 treatment was split roughly evenly between estimates of 3-cycles and 6-cycles (Fig. 8); the basic uncertainty arises because the value c_{pa} = 1.00 lies near a point where a 3-cycle bifurcates (recall Fig. 4).

Combinations of more complex behaviors were estimated for the c_{pa} = 0.00, 0.05, 0.10, and 0.35 treatments. At c_{pa} = 0.00, the spike of bootstrapped LE values at 0 in the histogram (Fig. 6) corresponds to the invariant loops (27%) indicated in the pie diagram (Fig. 8), while the negative LE values for that treatment (Fig. 6) were all stable 2-cycles (Fig. 8). Recall that the invariant loops in the ''point estimate'' of the attractor consisted of two tiny separate loops, producing trajectories resembling 2-cycles. For the c_{pa} = 0.05 treatment, 39.1% of the bootstrapped parameter sets gave chaotic attractors, and the remaining sets produced unusual stable cycles (Fig. 8). The c_{pa} = 0.10 treatment showed mostly stable cycles of unusual periods (e.g., 13-cycles). The c_{pa} = 0.35 treatment is our showcase for chaos. For that treatment, 83.5% of the bootstrapped parameter sets produced chaotic attractors, 7.1% produced stable 19-cycles, and the rest produced other stable cycles of higher periods (Fig. 8). In the unlikely

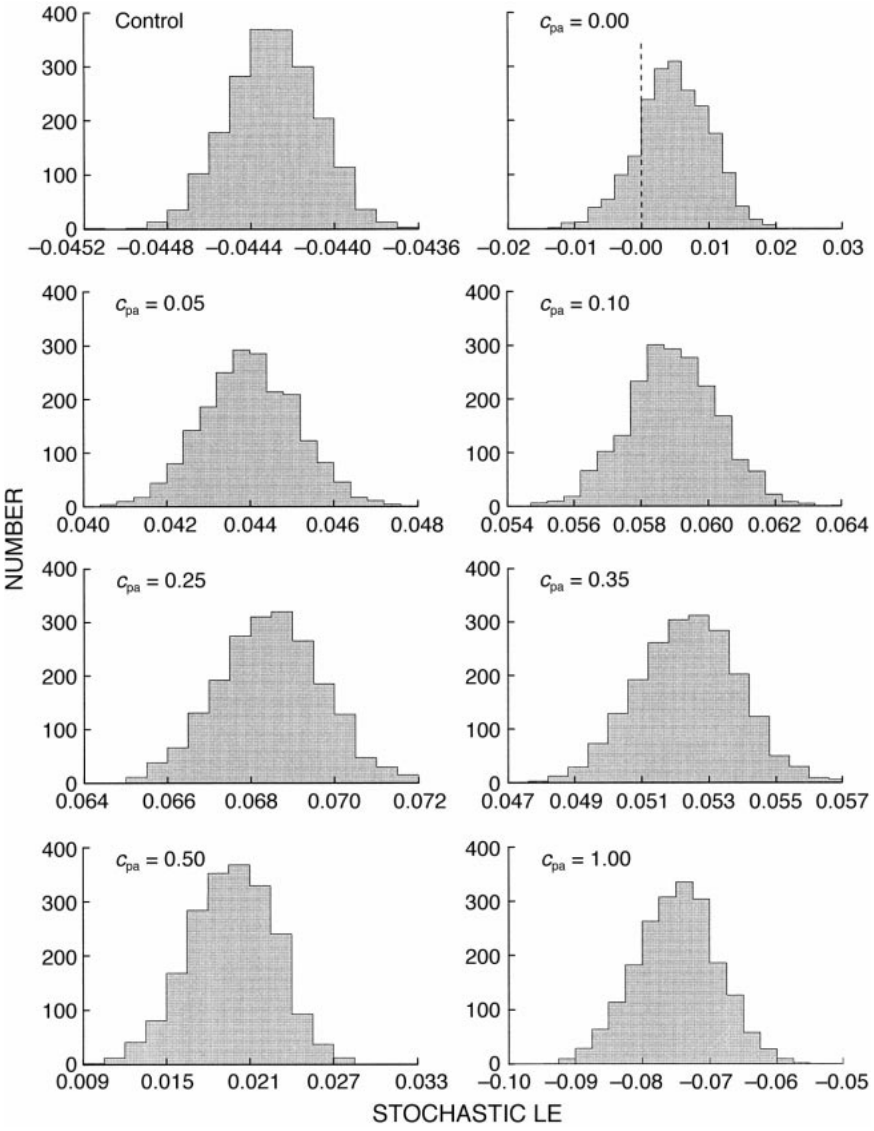

FIG. 7. Histograms of the 2000 bootstrap estimates of the stochastic Liapunov exponents (SLEs) for each experimental treatment.

possibility that the behavior of the $c_{pa} = 0.35$ treatment is a stable cycle, it would probably have a high period relative to the length of the time series ($q = 40$) and occur in a small periodic window of parameter space within a larger region of chaos (Fig. 5).

Model evaluation

The generalized R^2 values for the experimental populations were very high (Table 3). The L-stage (feeding larvae) R^2 values were generally lower than those for the P-stage (pupae and near pupae). While three of the L-stage R^2 values were between 0.4 and 0.5, twenty of them were above 0.75, and twelve were above 0.9. For the P-stage, only two R^2 values were below 0.9; both were for control populations. The lowest R^2 value for the P-stage in all of the treatment populations was 0.96 ($c_{pa} = 0.00$, replicate 15). Many treatment R^2 values for the P-stage were above 0.99. The greater variability of the L-stage is easy to interpret in that recruits arise from the intrinsically variable processes of egg-laying and egg survival. P-stage recruits, by contrast, arise through a simpler survival process (see Eq. 2). We did not report R^2 values for the A-stage (sexually mature adults) in the treatment cultures because the experimental manipulations render the treatment A-stage populations essentially deterministic. Note that the control populations have L-stages and P-stages that are more variable (lower R^2 values, on average) than those in the treatments; the additional variability stems from the unmanipulated adults in the controls.

Residual diagnostics indicate that the stochastic portion of the stochastic LPA model (Eqs. 10–12) is a

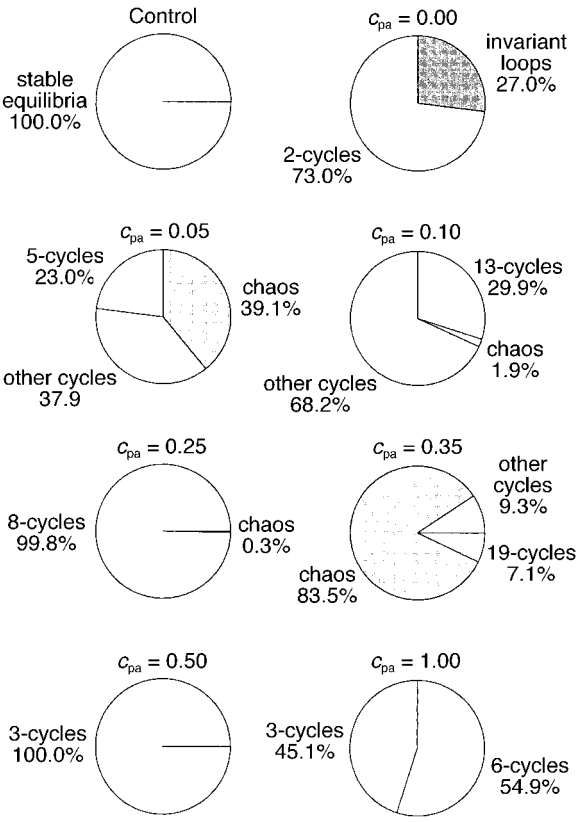

FIG. 8. Pie charts showing the frequency of predicted deterministic attractors at each treatment for the 2000 bootstrap parameter estimates.

TABLE 3. Fitted R^2 values for the life stages for each replicate.

Treatment	Replicate	Fitted R^2 L-stage	Fitted R^2 P-stage
Control	4	0.611	0.907
	11	0.456	0.859
	24	0.776	0.867
c_{pa} = 0.00	5	0.461	0.965
	12	0.776	0.972
	15	0.402	0.962
c_{pa} = 0.05	1	0.895	0.984
	7	0.905	0.985
	20	0.875	0.990
c_{pa} = 0.10	6	0.870	0.983
	10	0.873	0.990
	16	0.782	0.985
c_{pa} = 0.25	8	0.892	0.991
	17	0.923	0.983
	21	0.952	0.994
c_{pa} = 0.35	2	0.928	0.980
	13	0.962	0.995
	22	0.996	0.997
c_{pa} = 0.50	9	0.912	0.991
	14	0.959	0.995
	19	0.938	0.993
c_{pa} = 1.00	3	0.937	0.998
	18	0.948	0.990
	23	0.938	0.993
Overall		0.899	0.985

Notes: Life-cycle stages for *Tribolium*: ''L-stage'' means feeding larvae; ''P-stage'' includes large larvae, non-feeding larvae, pupae, and callow adults; and ''A-stage'' refers to sexually mature adults. The R^2 values for the A-stage in the control replicates are 0.996, 0.995, and 0.995 for replicates 4, 11, and 24, respectively, and the overall value in the controls is 0.996.

good representation of the noise in the data (Table 4). Significant first-order autocorrelation was detected in just 5 (10%) of the 51 time series for which there were residuals (L-, P-, and A-stages for 3 control populations, L- and P-stages for 21 treatment populations). Significant second-order autocorrelation was detected in just 7 (14%) of the time series; departure from a normal distribution was detected in 17 (33%) of the time series. These results are similar to results for 36 time series of this flour beetle strain (RR) reported for the first transitions experiment (3% first-order autocorrelated, 6% second-order autocorrelated, 33% nonnormal; Dennis et al. 1997). That two thirds of the residual time series would fail to show evidence of departure from normality is remarkable, given that the series are long enough ($q = 40$) for the normality test to have reasonable power (Lin and Mudholkar 1980). Various residual diagnostic plots, not reported here for space reasons, also showed excellent patterns (stable variances, normality). Note that the inferences we have made about parameters, dynamics, LE values, etc., are based on CLS estimation that makes no particular assumptions about the distributional form of the noise. The diagnostic tests and plots mainly suggest there are no major systematic or symptomatic patterns in the departures of model and data, allowing us to have greater confidence in the inferences made with the model.

That the estimated model skeleton accounts for a high degree of variability in the populations can be seen in time-series plots (Figs. 9 and 10). In Fig. 9, the L-, P-, and A-stage abundances are plotted for one representative population from the control and c_{pa} = 0.00, 0.05, and 0.10 treatments, along with the one-time-step forecasts of the fitted model. Fig. 10 gives the same plots for the c_{pa} = 0.25, 0.35, 0.50, and 1.00 treatments. The patterns of changes in dynamics and variability from treatment to treatment are captured well by the model, from the stable point equilibrium of the control, to the irregular behavior of c_{pa} = 0.35, to the strong periodic signals in the c_{pa} = 0.50 and 1.00 treatments. Occasionally the cyclic oscillations seemingly damp to a point equilibrium (for example, from $t = 8$ to $t = 16$ in the c_{pa} = 0.10 treatment, and from $t = 8$ to 19 in the c_{pa} = 1.00 treatment); the model in fact predicts such behavior in the form of transient ''flybys'' of an unstable equilibrium lying on a stable manifold (Cushing et al. 1998*b*).

Phase-space plots and stochastic simulations

The agreement of model and data can be visualized better in phase space. In the left columns of Fig. 11

TABLE 4. Residual analyses for each replicate. First-order ($\hat{\rho}_1$) and second-order ($\hat{\rho}_2$) sample autocorrelations and Lin-Mudholkar (z) test statistic for normality are reported.

Treatment	Replicate no.	L-stage			P-stage		
		$\hat{\rho}_1$	$\hat{\rho}_2$	z	$\hat{\rho}_1$	$\hat{\rho}_2$	z
Control†	4	0.47	0.27	1.40	−0.09	0.15	−0.96
	11	0.51	0.43	1.33	0.20	−0.09	2.14
	24	0.66	0.43	3.08	−0.07	0.22	1.81
$c_{pa} = 0.00$	5	0.24	0.04	2.24	0.15	−0.14	−0.19
	12	−0.29	0.19	1.72	−0.08	0.16	−0.17
	15	0.36	−0.12	2.78	0.03	0.23	−0.76
$c_{pa} = 0.05$	1	0.11	0.35	−1.82	−0.19	0.06	0.53
	7	−0.12	0.26	−0.13	−0.06	0.07	1.26
	20	−0.24	0.20	1.82	0.42	0.45	0.07
$c_{pa} = 0.10$	6	−0.23	0.29	1.09	−0.06	−0.33	0.69
	10	−0.24	0.41	−0.15	0.03	0.14	−0.28
	16	−0.17	0.00	−1.16	0.08	0.15	3.09
$c_{pa} = 0.25$	8	0.02	−0.24	−2.48	−0.17	0.04	−1.97
	17	−0.16	0.31	−2.12	0.08	0.04	3.53
	21	0.09	−0.05	2.51	−0.12	−0.02	−0.65
$c_{pa} = 0.35$	2	−0.03	0.29	−1.12	−0.05	−0.03	−3.60
	13	0.01	0.11	0.00	−0.00	−0.20	−1.13
	22	−0.04	0.19	0.68	0.13	−0.16	−2.57
$c_{pa} = 0.50$	9	−0.18	−0.06	−2.45	−0.12	−0.05	2.16
	14	0.16	−0.14	0.28	−0.12	0.14	1.45
	19	−0.12	0.09	−0.58	−0.06	−0.09	−1.40
$c_{pa} = 1.00$	3	0.10	0.16	0.49	0.03	0.05	−2.24
	18	0.20	0.27	−0.64	−0.02	−0.11	1.66
	23	0.11	0.19	0.87	−0.09	−0.03	2.17

Notes: There is significant (0.05 level of probability) jth-order autocorrelation if $|\hat{\rho}_j|$ exceeds 0.31. There is significant (0.05 level of probability) departure from normality if $|z|$ exceeds 1.96. The diagnostic statistics for the A-stage residuals of the control treatments are: $\hat{\rho}_1 = 0.26$, $\hat{\rho}_2 = 0.23$, $z = -2.10$ for replicate 4; $\hat{\rho}_1 = -0.00$, $\hat{\rho}_2 = -0.02$, $z = 1.18$ for replicate 11; and $\hat{\rho}_1 = 0.14$, $\hat{\rho}_2 = 0.01$, $z = 2.11$ for replicate 24.

(A, C, E, G) and Fig. 12 (A, C, E, G), we plotted the data triples $[l_t, p_t, a_t]$ from each treatment in phase space after removing initial transient observations. Open circles are the data points; the dark circles or lines represent the estimated stable attractor for that treatment. The model attractors capture the transitions in dynamic behavior of the data from treatment to treatment extremely well. Note the tight cloud of points around the stable point equilibrium for the control treatment (Fig. 11A), the two clouds of points around the small invariant loops for the $c_{pa} = 0.00$ treatment (Fig. 11C), the irregular, triangular-shaped clouds of data points that accompany the three-pointed cyclic or chaotic attractor of the $c_{pa} = 0.05$, 0.10, 0.25, and 0.35 treatments (Figs. 11E and G, 12A and C), and the clustering of points around the 3-cycle and 6-cycle of the $c_{pa} = 0.50$ and 1.00 treatments (Fig. 12E and G).

Clearly the data in Figs. 11 (A, C, E, G) and 12 (A, C, E, G) are influenced strongly by the deterministic forces present in the model. Also, there are clear departures of data from model. Does the variability predicted by the stochastic model resemble the variability in the data? The right columns of Figs. 11 and 12 (B, D, F, H) depict stochastic triples simulated using the estimated stochastic model (Eqs. 10–12, with parameter values given by Table 1), with initial transients removed. For the purpose of the simulations, the noise vector $\mathbf{E}_t$ was assumed to have a multivariate normal distribution (recall that multivariate normality was not assumed for the estimation methods). The simulations are thus shown side by side with the corresponding data for each treatment. The resemblance of the left and right plots for each treatment is striking. The stochastic model produced cloud patterns of observations around the estimated attractors that can hardly be distinguished visually from the data. In ecology, such concordance of model and data across experimental manipulations is rare.

DISCUSSION

Asymptotic dynamics and stochasticity

Asymptotic dynamics (''final states'') such as equilibria, cycles, and chaos are deterministic mathematical notions defined in terms of equations and arbitrarily large temporal extents. Physical systems, being temporally finite, do not have asymptotic properties. Even so, these precise mathematical notions are useful for describing and understanding physical systems. (Indeed, the mathematical notions are perhaps nothing more than idealized abstractions gleaned from the observation of physical systems.) While a physical system cannot be at equilibrium, or on a limit cycle, or chaotic in a strict mathematical sense, these model concepts are useful as approximations to physical reality. If the state of a physical system is well described by a de-

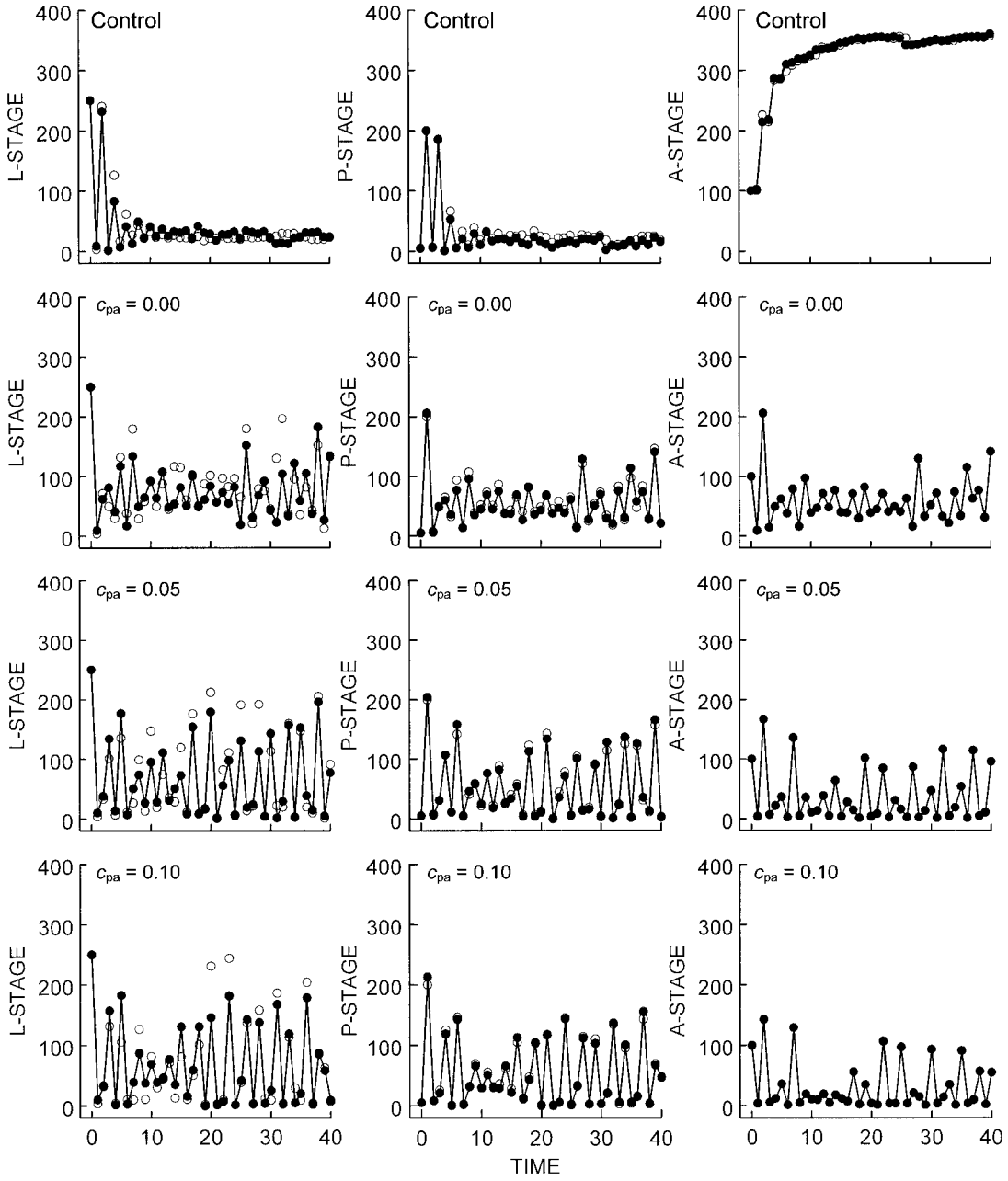

FIG. 9. Time-series data (●) and one-step predictions from the fitted model (○) for representative cultures from four experimental treatments: control, and c_{pa} (adult–pupa cannibalism coefficient) = 0.00, 0.05, and 0.10. The unit of time is two weeks.

terministic model, investigators commonly ascribe the mathematical dynamic of the model to the system. However, in population systems the role of chaos and other deterministic nonlinear dynamic behaviors, both asymptotic and transient, must be understood in the context of stochasticity.

Ecological populations are stochastic. Observed time series, from completely censused laboratory populations cultured under near-constant environmental conditions (Costantino and Desharnais 1981, Dennis and Costantino 1988) to extensive field surveys of population abundances (Woiwod and Hanski 1992), are characterized by pervasive, unexplained noise. In an analysis of 59 laboratory and field time-series data sets, Ellner and Turchin (1995) found that low-dimensional deterministic dynamics seldom accounted for more than half of the total variability in the data. While incorporation of weather covariates in time series (Roth-

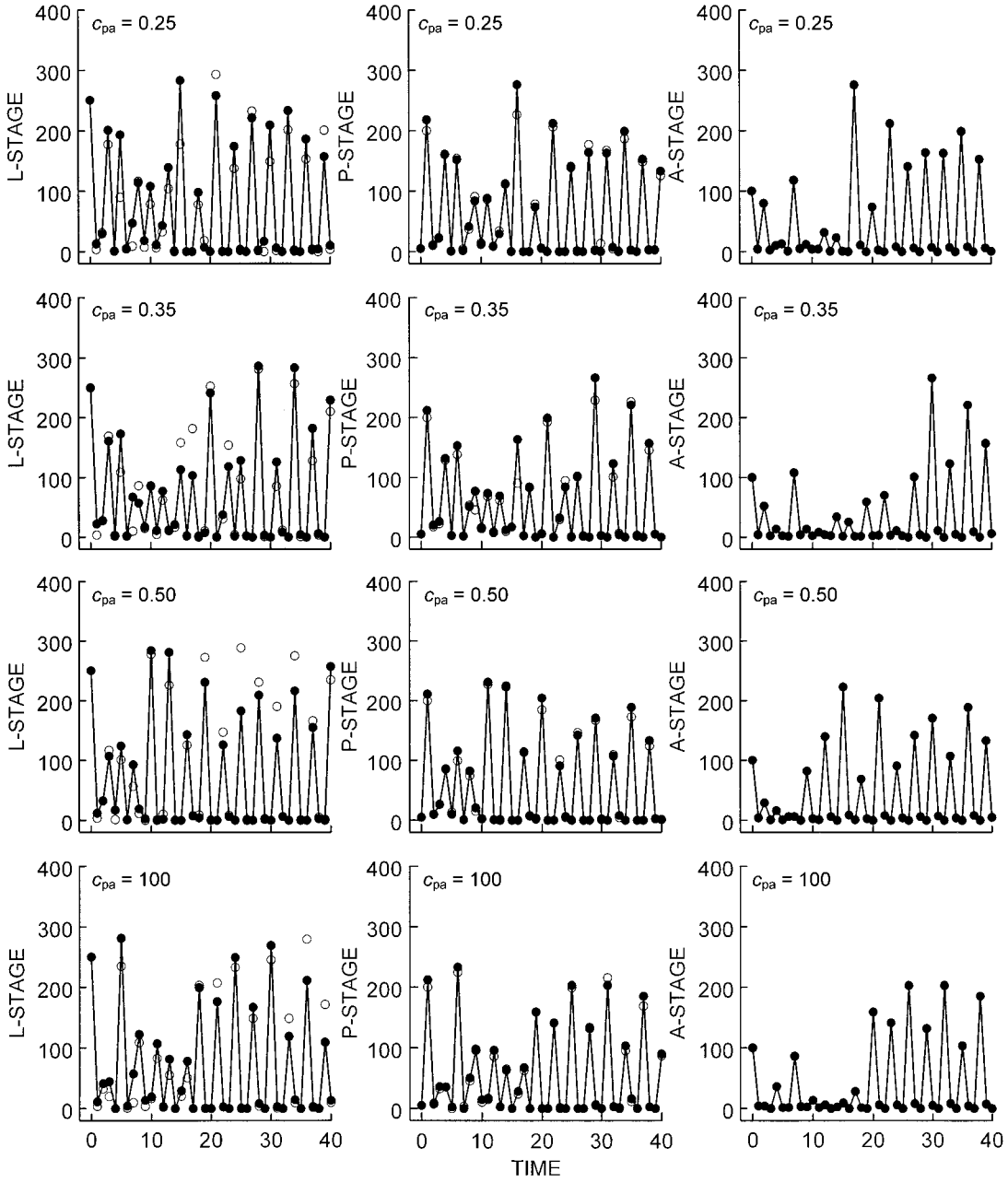

FIG. 10. Time-series data (●) and one-step predictions from the fitted model (○) for representative cultures from four experimental treatments: c_{pa} = 0.25, 0.35, 0.50, and 1.00. The unit time is two weeks.

ery et al. 1997, Dennis and Otten 2000) will potentially account for some of the unexplained variability in field populations, population ecologists are a long way from being able to rely on ''laws'' of population dynamics in the form of differential or difference equations.

Noise in ecological systems has three major impacts on attempts to build appropriate mathematical models of population dynamics and to interpret population behavior in terms of model dynamic behavior. First, the noise must be included as an integral part of the model. Second, model parameters, and the resulting model dynamics, are estimated with statistical uncertainty. Third, the noise fundamentally alters the dynamic behaviors of the model. We discuss each of these impacts in turn, with reference to our results.

1. *Modeling the noise*.—If mathematical population models are to be built and tested as serious scientific hypotheses, the models must somehow be connected to data. Such connection implies that the noise must be modeled, in order to construct an appropriate estimating function for the model parameters (based on likelihood or conditional sums of squares, for instance).

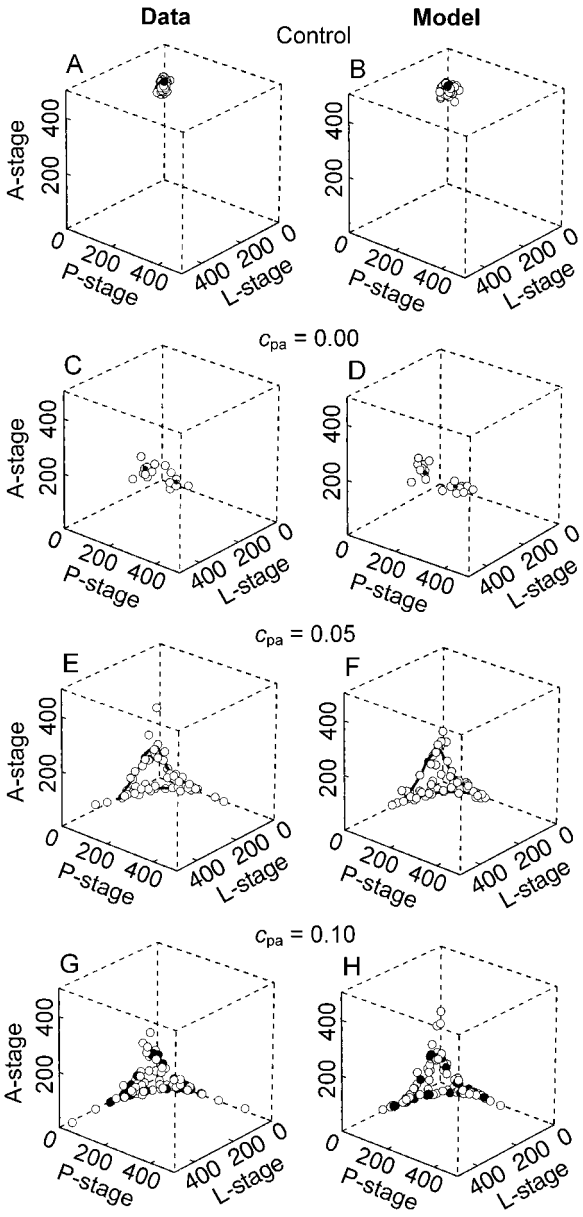

FIG. 11. Phase-space plots for the data (○ in A, C, E, G) and stochastic model (○ in B, D, F, H) for weeks 40–80 together with the predicted deterministic attractor (● or lines) for four experimental treatments: control, and c_{pa} = 0.00, 0.05, and 0.10. The values from the stochastic model were generated from simulations with the same initial conditions, number of replicates, and length of time series as the experimental data. The week 0–38 observations for the control and c_{pa} = 0.05 and 0.10 treatments were discarded to focus attention on the asymptotic attractors. The week 0–66 observations for the c_{pa} = 0.00 treatment were discarded since simulations indicated that this treatment exhibits longer transients.

The noise model component should be evaluated with data, using statistical diagnostic procedures. There is reason for encouragement; recent studies suggest that constructing useful stochastic models is feasible for various ecological systems. In at least some studies, diagnostic analyses of fitted models revealed noise with a simple probabilistic structure, such as a normal distribution (Dennis and Costantino 1988, Dennis et al. 1991, 1995, 1998, Kemp and Dennis 1993, Dennis and Taper 1994).

In the present study, the departures of data from the model skeleton were well described by a model of demographic variability. We hypothesized that the survival of a cohort of flour beetles through a life stage would resemble a simple binomial random process, and that recruitment of small larvae would be similar to a Poisson distribution. The binomial or Poisson-distribution parameters were modeled as nonlinear functions of the state variables in such a way that the mean trend for the system predicted over one time unit was the deterministic LPA model. The binomial and Poisson distributions had the property that the stochastic variability would appear as approximately normally distributed ''noise'' on the square-root scale. In the 24 experimental populations, the normal noise model provided overall an excellent description of the residual variation in the populations after the nonlinear effects predicted by the LPA model had been estimated and accounted for in the time series.

2. *Estimating the dynamics*.—When models are connected to data and parameters are appropriately estimated, interpretations of dynamic population behavior come with ''confidence intervals.'' In an earlier study, using a different strain of flour beetle, we displayed a joint parameter confidence region for unmanipulated control populations that contained stable 2-cycles as well as stable points (Dennis et al. 1995: Fig. 3). When a confidence region contains chaos, the situation can be far more complicated. Even though a point estimate of deterministic model parameters corresponds to a chaotic regime, a bewildering variety of other dynamic states could be embedded in the parameter confidence region. In fact, it was informative in the present study to divide the entire estimated sampling distribution of the parameter estimates into ''confidence sets,'' in which a degree of confidence is associated with a particular type of dynamic behavior. For instance, we are 39% confident that the c_{pa} = 0.05 treatment has a skeleton with a chaotic attractor, 23% confident that the attractor is a 5-cycle, and 38% confident that the attractor is cyclic with some other period (Fig. 8).

Based on our stochastic model and estimation procedures, we are 83.5% confident that the c_{pa} = 0.35 treatment has an underlying chaotic attractor, and 16.5% confident that the attractor is an unusual high-period cycle such as a 19-cycle (Fig. 8). The confidence sets provide strong support for our claim that the fluctuations of the c_{pa} = 0.35 treatment populations are largely explained by complex nonlinear behavior arising from simple, known population forces.

3. *Emergent dynamic behavior*.—Noise combines with deterministic forces to produce emergent dynamic

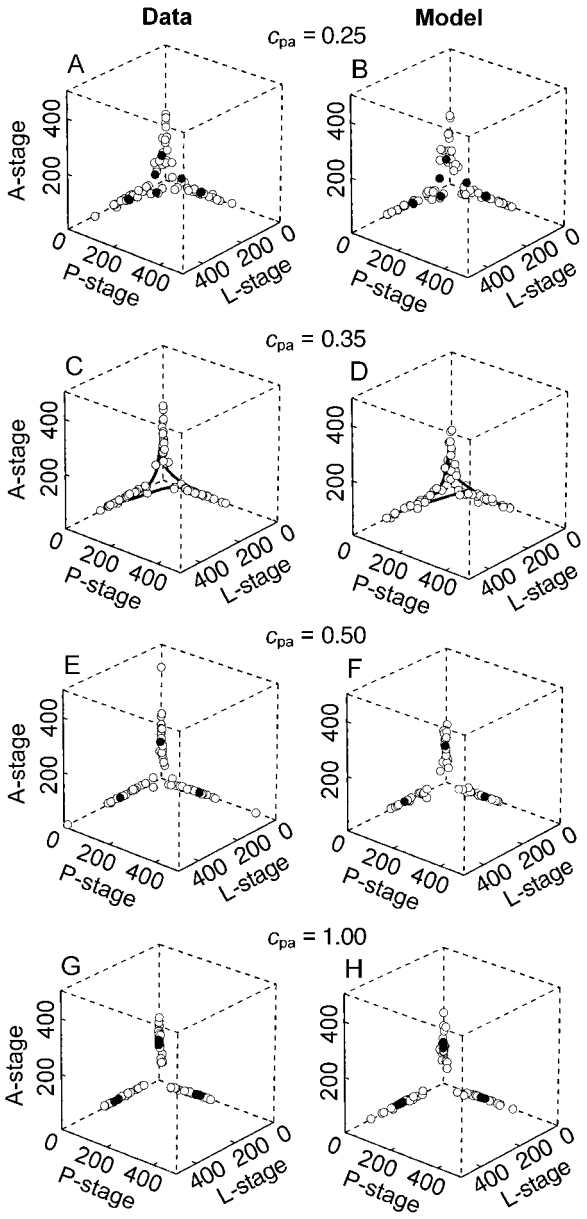

FIG. 12. Phase-space plots for the data (○ in A, C, E, G) and stochastic model (○ in B, D, F, H) for weeks 40–80 together with the predicted deterministic attractor (● or lines) for four experimental treatments: c_{pa} = 0.25, 0.35, 0.50, and 1.00. The values from the stochastic model were generated from simulations with the same initial conditions, number of replicates, and length of time series as the experimental data. The week 0–38 observations were discarded to focus attention on the asymptotic attractors.

behaviors. Indeed, the mathematical notions of stability, periodicity, and chaos defined for deterministic systems do not strictly apply to stochastic systems. Instead of a chaotic stochastic system, or a periodic stochastic system, it is more appropriate to speak of the *influence* of a chaotic or periodic skeleton on the stochastic system. The skeleton and the noise together determine the dynamics (Leirs et al. 1997); the skeleton merely influences the dynamics.

The NLAR (nonlinear autoregressive) model (Eq. 9) can serve as a multivariate stochastic version of many types of ecological population models (Dennis et al. 1995, 1998), under demographic (square-root scale) or environmental (log scale) stochasticity. Such models have emergent dynamic properties that must temper discussions of nonlinear dynamics in ecology.

3a. *The attractor of an NLAR model is a stationary probability distribution*.—The stationary distribution, if it exists, gives the long-run proportion of time that the system spends in a region of phase space as an integral of the stationary probability density function over that region. The population trajectories under Eq. 9 typically do not become confined to a reduced-dimension set, such as a point, cycle, or strange attractor. Rather, all regions of phase space are eventually visited. The stationary probability density function is typically smooth, instead of fractal like the invariant measure of a strange attractor, though the density might have many modes.

The stationary distribution for the stochastic LPA model (Eqs. 10–12) was estimated to undergo distinctive changes in response to our experimental manipulations of adult recruitment and mortality. The distributions under the different experimental treatments were manifested in model simulations as clouds of points around underlying deterministic attractors (Figs. 11 and 12). The resemblance of the model and data clouds, in particular the degree of variability around the attractors and the responses of the cloud patterns to the treatments, was striking (Figs. 11 and 12). Most of the probability in these stationary distributions was concentrated near the underlying attractors, suggesting that the attractors strongly influence the stochastic-model dynamics. Identifying the best statistical methods for comparing these fitted, exotic multivariate distributions with data is an open question that we are currently researching.

3b. *Transient phenomena recur*.—Noise continually stirs stochastic systems, knocking trajectories away from the attractors of the skeleton. Transient phenomena, such as visitation to the neighborhood of an unstable equilibrium, eventually recur. Sometimes an unstable point (or other invariant sets such as an unstable cycle or fractal set) resides on a reduced-dimensional stable manifold, so that trajectories near the manifold tend to move toward the unstable point before moving away toward a stable attractor (Cushing et al. 1998*b*). The effect is for trajectories in the stochastic system to display occasional ''fly-bys'' of divergence regions of phase space, followed by fresh transient returns to the attracting region. As noted earlier (see *Results: Model evaluation*), recurring fly-bys of an unstable point equilibrium are evident in time series reported in the present study (Fig. 10). Long-run time spent near divergence regions is accounted for in the stationary

distribution. This recurring divergence implies a sensitivity to initial conditions of a kind fundamentally different from deterministic chaos (see Rand and Wilson 1991).

3c. *Noise can cause transitions between multiple deterministic final states*.—Stochasticity, in conjunction with the presence of unstable invariant separatrix sets and the nature, location, and size of basins of attraction, can ''bump'' model trajectories from one attracting deterministic state to another. For example, noise may cause a cycle to shift phase (Henson et al. 1998) or, in a regime with multiple deterministic attractors, may cause an orbit to jump from one cyclic attractor to another (Henson et al. 1999).

Influence of chaos on ecological populations

In a strict mathematical sense, populations cannot be chaotic for three reasons. First, even if populations were not stochastic, they are of finite temporal extent and thus do not have asymptotic dynamics such as equilibria or chaos. Second, given that populations are stochastic, the dynamics of their models must be estimated with confidence intervals, in which may be embedded dynamics other than chaos. Third, because of the interactions of stochasticity and deterministic influences, populations are not confined to a chaotic attractor so long as even a little stochasticity is present.

Instead, a more realistic hypothesis for a particular population might be that the population fluctuations are strongly influenced by a skeleton with, say, a strange attractor. Indeed, they might be strongly influenced by an unstable chaotic set through recurring transient behavior near the set. If so, then useful understandings and predictions might be accomplished with models that combine deterministic and stochastic aspects, and that is what we have demonstrated here.

Furthermore, an important take-home message of nonlinear dynamics for ecologists is not chaos per se, but rather that systems can undergo transitions among different types of behaviors in response to changing conditions, and that these transitions might be predicted with suitable stochastic models. Our experiments were designed around a specific sequence of transitions predicted by a promising biological model. A chaotic skeleton was predicted to be sandwiched between characteristic cyclic or stable-point skeletons, like books between bookends, along a range of values of a control parameter. The model predicted that the skeletons were influential enough that the transitions would be observed in experimental populations in response to manipulations of the control parameter value. The overall R^2 values indicated that the fitted LPA skeleton accounted for 89.9% of the L-stage (feeding larvae) variability and 98.5% of the P-stage (between feeding larvae and sexually mature adults; pupae) variability in the experimental populations (Table 3). The data plotted in phase space showed clear transitions in behavior and closely matched the predicted cycles on either side and the predicted strange attractor in the middle.

Are any of the populations in this experiment *influenced* by chaotic dynamics? On the basis of the point estimates of the Liapunov exponents (LEs) (see Table 2), the deterministic attractors for the c_{pa} (i.e., the adult pupa cannibalism coefficient) = 0.05 and 0.35 treatments are chaotic. There is additional supporting evidence. Histograms of the bootstrap estimates of the LEs revealed the occurrence of positive values for both treatments (Fig. 6), with the frequencies of positive values being 39.1% and 83.5% for the c_{pa} = 0.05 and 0.35 populations, respectively (Fig. 8). Bootstrapped bifurcation diagrams placed both treatments in regions of complex dynamic behavior interwoven with chaos and high-period cycles (Fig. 4). The deterministic skeleton accounted for 92.5% of the variability in the (transformed) L-stage abundances, and 98.9% of the P-stage abundances, in the six cultures allotted to the c_{pa} = 0.05 and 0.35 treatments, according to the generalized R^2 value calculated for those populations. We conclude that the c_{pa} = 0.05 and 0.35 populations are strongly influenced by chaotic dynamics.

Sensitivity to initial conditions

Sensitivity to initial conditions is a hallmark of deterministic chaos. In a deterministic system, such sensitivity is a straightforward concept, and is widely measured with the dominant LE. The LE is the early divergence rate of two trajectories that differ infinitesimally in initial conditions, averaged over the system attractor (point, cycle, strange attractor, etc.). The average is taken with respect to the invariant measure of the attractor. The deterministic attractor is generally a set of greatly reduced dimension in phase space. Conditions on the attractor (where the LE is calculated) do not typify conditions elsewhere in phase space. The estimated LEs of the LPA model skeleton were positive at c_{pa} = 0.05 and 0.35 (Table 2, Fig. 3B), indicating that for these c_{pa} values the skeleton alone produces chaotic behavior, that is, trajectories on the predicted strange attractor have the property (on average) of sensitivity to initial conditions.

Sensitivity to initial conditions must be measured in some other fashion, however, for a stochastic system. As is clear from both model simulations and data, stochastic trajectories at c_{pa} = 0.05 and 0.35 do not spend much time actually on the attractors, but do behave as if influenced by the attractor (Figs. 11 and 12). Do such trajectories, in their recurrent visitations of transient areas of phase space, have the sensitivity property? It depends on how that sensitivity is defined.

The definition embodied in the ''stochastic LE'' (SLE) averages the trajectory divergence rate over the stationary distribution. The average can be calculated from the ergodic property by taking a time average of the divergence rate over a single long trajectory (see *Appendix*, and also Ellner and Turchin 1995). This def-

inition, proposed by Crutchfield et al. (1982) and studied and advocated by McCaffrey et al. (1992), would seem a natural extension of the deterministic sensitivity concept to stochastic systems. Indeed, the SLEs calculated for $c_{pa} = 0.05$ and 0.35 (Table 2, Fig. 3C) indicate that trajectories of the predicted stochastic model for these c_{pa} treatments have, on average, the sensitivity property, so defined.

According to the full stochastic model, the $c_{pa} = 0.00$, 0.10, 0.25, and 0.50 treatments are also predicted to have the sensitivity property; the SLEs are positive. At first glance the situation might appear peculiar: the skeleton of the model for each of these c_{pa} values is decidedly nonchaotic, while the full stochastic model shows sensitivity to initial conditions. Is the noise somehow causing sensitivity to initial conditions?

The explanation lies in the properties of the stochastic NLAR model (Eq. 9). The stationary distribution accounts for the long-run time spent in all portions of phase space, including regions of phase space where initially close trajectories governed by the skeleton tend to diverge. In some situations a significant proportion of time can be spent by a stochastic system in a divergence region; if such a system is allowed to run for a long time and then stopped at random and observed, chances are fair by the ergodic property that the system will be in a divergence region. If a positive SLE were taken as a definition of chaos, then noise could ''induce chaos'' by continually knocking the system into phase-space regions that are transient and locally diverging according to the skeleton.

In fact, it is possible to construct a stochastic logistic/Ricker model in which the skeleton predicts a critically damped, globally stable point equilibrium, yet the SLE is positive (Desharnais et al. 1997). The noise in the model frequently places the population at low abundance levels, well below the stable point equilibrium of the skeleton. Because zero is an unstable equilibrium, trajectories near it diverge (growing approximately exponentially toward the stable equilibrium point). While such a system displays, on average, ''sensitivity to initial conditions,'' it is not clear that population ecologists would want to label such a system ''chaotic.'' After all, noisy perturbation around a stable equilibrium is a leading alternative hypothesis to chaos concerning the nature of fluctuations in natural populations (Pool 1989*a*, *b*).

Thus, defining chaos in terms of a positive SLE confounds both stochasticity and complex nonlinear dynamics; it classifies noisy systems as chaotic as well as systems under the influence of low-dimensional, nonlinear forces. Instead, we find studying and quantifying the influence of biologically based model skeletons useful for identifying the role of nonlinear dynamics in population ecology. All along, the mathematical chaos theorists provocatively suggested that population fluctuations might be largely deterministic, possibly caused by simple but unidentified nonlinear interactions (May and Oster 1976). In other words, it was hypothesized that if some underlying deterministic skeleton could be identified correctly, then the population fluctuations might be substantially explained and understood. Because of the presence of noise, ecological populations cannot be strictly chaotic; however, there remains the prospect that some ecological populations can be strongly influenced by underlying deterministic forces.

We have demonstrated that experimental *Tribolium* populations are strongly influenced by dynamics contained within a simple nonlinear skeleton. The predictions of the skeleton accounted for most of the variability of L-stage and P-stage numbers of 24 experimental populations. Furthermore, the skeleton forecasted substantially different dynamics depending on the experimental treatments, and these different dynamic transitions were displayed by the experimental populations. For the treatments with parameter c_{pa} experimentally set at 0.05 and 0.35, the estimated skeleton predicted chaotic dynamics. The skeleton accounted for most of the variability of L-stage and P-stage abundances displayed by the three populations at the $c_{pa} = 0.05$ and 0.35 treatments. The statistical patterns in the leftover noise were well described by a model of demographic stochastic forces.

Concluding Remarks

While there is no such thing as strict mathematical chaos—or even equilibria or cycles—in biological populations, ecologists can be encouraged that simple nonlinear models can help unlock substantial gains in understanding population systems. Keys to transforming nonlinear models from scientific caricatures to testable scientific hypotheses are: (a) incorporating the noise as well as the signal in biologically based models, (b) explicitly connecting models and data, (c) focusing on statistics as well as mathematics, (d) focusing on real systems and observable state variables, (e) rigorously evaluating model performance, and (f) effectively combining biology, mathematics, and statistics in interdisciplinary teamwork. As always, a well-designed experiment can pose a strong challenge to a model and help cut through a confusing fog of alternative possibilities. The *Tribolium* system has been studied and modeled in ecology for over 70 yr. We are just beginning to attain a mathematical understanding of its workings and a new appreciation of its possibilities.

Acknowledgments

This research was supported in part by U.S. National Science Foundation grants DMS-9625576 and DMS-9616205. The paper benefited greatly from the suggestions of Roger Nisbet (subject-matter editor) and two anonymous referees. This paper is contribution number 914 of the Forest, Wildlife, and Range Experiment Station of the University of Idaho.

Literature Cited

Alligood, K. T., T. D. Sauer, and J. A. Yorke. 1997. Chaos: an introduction to dynamical systems. Springer-Verlag, Berlin, Germany.

Ascioti, F. A., E. Beltrami, T. O. Carroll, and C. Wirick. 1993. Is there chaos in plankton dynamics? Journal of Plankton Research **15**:603–617.

Bailey, B. S. A., S. Ellner, and D. W. Nychka. 1997. Chaos with confidence: asymptotics and applications of local Lyapunov exponents. Pages 115–133 *in* C. Cutter and D. J. Kaplan, editors. Nonlinear dynamics and time series: building a bridge between the natural and statistical sciences. American Mathematical Society, Providence, Rhode Island, USA.

Bartlett, M. S. 1990. Chance or chaos? (with discussion). Journal of the Royal Statistical Society **A52**:321–347.

Begon, M., S. M. Sait, and D. J. Thompson. 1996. Predator–prey cycles with period shifts between two- and three-species systems. Nature **381**:311–315.

Benoît, H. P., E. McCauley, and J. R. Post. 1998. Testing the demographic consequences of cannibalism in *Tribolium confusum*. Ecology **79**:2839–2851.

Bjornstad, O., M. Begon, N. C. Stenseth, W. Falck, S. M. Sait, and D. J. Thompson. 1998. Population dynamics of the Indian meal moth: demographic stochasticity and delayed regulatory mechanisms. Journal of Animal Ecology **67**:110–126.

Boswell, M. T., J. K. Ord, and G. P. Patil. 1979. Chance mechanisms underlying univariate distributions. Pages 3–156 *in* J. K. Ord, G. P. Patil, and C. Taillie, editors. Statistical distributions in ecological work. International Cooperative Publishing House, Fairland, Maryland, USA.

Chan, K. S., and H. Tong. 1994. A note on noisy chaos. Journal of the Royal Statistical Society **B56**:301–311.

Cipra, B. 1999. Beetlemania: chaos in ecology. Pages 72–81 *in* P. Zorn, editor. What's happening in the mathematical sciences 1998–1999. Volume 4. American Mathematical Society, Providence, Rhode Island, USA.

Costantino, R. F., J. M. Cushing, B. Dennis, and R. A. Desharnais. 1995. Experimentally induced transitions in the dynamic behavior of insect populations. Nature **375**:227–230.

Costantino, R. F., J. M. Cushing, B. Dennis, R. A. Desharnais, and S. M. Henson. 1998. Resonant population cycles in temporally fluctuating habitats. Bulletin of Mathematical Biology **60**:247–273.

Costantino, R. F., and R. A. Desharnais. 1981. Gamma distributions of adult numbers for *Tribolium* populations in the region of their steady states. Journal of Animal Ecology **50**:667–681.

Costantino, R. F., R. A. Desharnais, J. M. Cushing, and B. Dennis. 1997. Chaotic dynamics in an insect population. Science **275**:389–391.

Crutchfield, J. P., J. D. Farmer, and B. A. Huberman. 1982. Fluctuations and simple chaotic dynamics. Physics Reports **92**:45–82.

Cushing, J. M., R. F. Costantino, B. Dennis, R. A. Desharnais, and S. M. Henson. 1998*a*. Nonlinear population dynamics: models, experiments and data. Journal of Theoretical Biology **194**:1–9.

Cushing, J. M., B. Dennis, R. A. Desharnais, and R. F. Costantino. 1996. An interdisciplinary approach to understanding nonlinear ecological dynamics. Ecological Modelling **92**:111–119.

Cushing, J. M., B. Dennis, R. A. Desharnais, and R. F. Costantino. 1998*b*. Moving toward an unstable equilibrium: saddle nodes in population systems. Journal of Animal Ecology **67**:298–306.

Cushing, J. M., S. M. Henson, R. A. Desharnais, B. Dennis, R. F. Costantino, and A. King. 2001. A chaotic attractor in ecology: theory and experimental data. Chaos, Solitons, and Fractals **12**:219–234.

Dennis, B., and R. F. Costantino. 1988. Analysis of steady-state distributions with the gamma abundance model: application to *Tribolium*. Ecology **69**:1200–1213.

Dennis, B., R. A. Desharnais, J. M. Cushing, and R. F. Costantino. 1995. Nonlinear demographic dynamics: mathematical models, statistical methods, and biological experiments. Ecological Monographs **65**:261–281.

Dennis, B., R. A. Desharnais, J. M. Cushing, and R. F. Costantino. 1997. Transitions in population dynamics: equilibria to periodic cycles to aperiodic cycles. Journal of Animal Ecology **66**:704–729.

Dennis, B., W. P. Kemp, and M. L. Taper. 1998. Joint density dependence. Ecology **79**:426–441.

Dennis, B., P. L. Munholland, and J. M. Scott. 1991. Estimation of growth and extinction parameters for endangered species. Ecological Monographs **61**:115–143.

Dennis, B., and M. R. M. Otten. 2000. Joint effects of density dependence and rainfall on abundance of San Joaquin kit fox. Journal of Wildlife Management **64**:388–400.

Dennis, B., and M. L. Taper. 1994. Density dependence in time series observations of natural populations: estimation and testing. Ecological Monographs **64**:205–224.

Desharnais, R. A., and R. F. Costantino. 1980. Genetic analysis of a population of *Tribolium*. VII. Stability: response to genetic and demographic perturbations. Canadian Journal of Genetics and Cytology **22**:577–589.

Desharnais, R. A., R. F. Costantino, J. M. Cushing, and B. Dennis. 1997. Estimating chaos in an insect population. Science **276**:1881–1882.

Dixon, P. A., M. J. Milicich, and G. Sugihara. 1999. Episodic fluctuations in larval supply. Science **283**:1528–1530.

Ellner, S. 1991. Detecting low-dimensional chaos in population dynamics data: a critical review. Pages 63–91 *in* J. A. Logan and F. P. Haines, editors. Chaos and insect ecology. Virginia Experiment Station Information Series 91-3. Virginia Polytechnic Institute and State University, Blacksburg, Virginia, USA.

Ellner, S., and P. Turchin. 1995. Chaos in a noisy world: new methods and evidence from time-series analyses. American Naturalist **145**:343–375.

Falck, W., O. N. Bjornstad, and N. C. Stenseth. 1995*a*. Bootstrap estimated uncertainty of the dominant Lyapunov exponent for Holarctic microtine rodents. Proceedings of the Royal Society of London **B261**:159–165.

Falck, W., O. N. Bjornstad, and N. C. Stenseth. 1995*b*. Voles and lemmings: chaos and uncertainty in fluctuating populations. Proceedings of the Royal Society of London **B262**: 363–370.

Finkenstadt, B., M. Keeling, and B. Grenfell. 1998. Patterns of density dependence in measles dynamics. Proceedings of the Royal Society of London **B265**:753–762.

Godfray, H. C. J., and S. P. Blythe. 1990. Complex dynamics in multispecies communities. Philosophical Transactions of the Royal Society of London **B330**:221–233.

Godfray, C., and B. T. Grenfell. 1993. The continuing quest for chaos. Trends in Ecology & Evolution **8**:43–44.

Godfray, C., and M. Hassell. 1997. Chaotic beetles. Science **275**:323–324.

Grenfell, B. T., A. Kleczkowski, S. P. Ellner, and B. M. Bolker. 1994. Measles as a case-study in nonlinear forecasting and chaos. Philosophical Transactions of the Royal Society of London **A348**:515–530.

Hassell, M. P., H. N. Comins, and R. M. May. 1991. Spatial structure and chaos in insect population dynamics. Nature **353**:255–258.

Hassell, M. P., J. H. Lawton, and R. M. May. 1976. Patterns of dynamical behaviour in single-species populations. Journal of Animal Ecology **45**:471–486.

Hastings, A., C. L. Hom, S. Ellner, P. Turchin, and H. C. J. Godfray. 1993. Chaos in ecology: Is mother nature a strange attractor? Annual Review of Ecology and Systematics **24**:1–33.

Henson, S., R. F. Costantino, J. M. Cushing, B. Dennis, and R. A. Desharnais. 1999. Multiple attractors, saddles, and

population dynamics in periodic habitats. Bulletin of Mathematical Biology **61**:1121–1149.
Henson, S., J. M. Cushing, R. F. Costantino, B. Dennis, and R. A. Desharnais. 1998. Phase switching in population cycles. Proceedings of the Royal Society of London **B265**: 2229–2234.
Higgens, K., A. Hastings, J. N. Sarvela, and L. W. Botsford. 1997. Stochastic dynamics and deterministic skeletons: population behavior of Dungeness crab. Science **276**:1431–1435.
Ives, A. R., J. Foufopoulos, D. Klopfer, J. L. Krug, and T. M. Palmer. 1996. Bottle or big-scale studies: How do we do ecology? Ecology **77**:681–685.
Kareiva, P. 1989. Renewing the dialogue between theory and experiments in population ecology. Pages 68–88 *in* J. Roughgarden, R. M. May, and S. A. Levin, editors. Perspectives in ecological theory. Princeton University Press, Princeton, New Jersey, USA.
Kareiva, P. 1995. Predicting and producing chaos. Nature **375**:189–190.
Kemp, W. P., and B. Dennis. 1993. Density dependence in rangeland grasshoppers (Orthoptera: Acrididae). Oecologia **96**:1–8.
Kendall, B. E., C. J. Briggs, W. W. Murdoch, P. Turchin, S. P. Ellner, E. McCauley, R. M. Nisbet, and S. N. Wood. 1999. Why do populations cycle? A synthesis of statistical and mechanistic modeling approaches. Ecology **80**:1789–1805.
Kifer, Y. 1986. Ergodic theory of random transformations. Birkhauser, Boston, Massachusetts, USA.
Klimko, L. A., and P. I. Nelson. 1978. On conditional least squares estimation for stochastic processes. Annals of Statistics **6**:629–642.
Leger, C., D. N. Politis, and J. P. Romano. 1992. Bootstrap technology and applications. Technometrics **34**:378–398.
Lehmann, E. 1983. Theory of point estimation. John Wiley & Sons, New York, New York, USA.
Leirs, H., N. C. Stenseth, J. D. Nichols, J. E. Hines, R. Verhagen, and W. Verheyen. 1997. Stochastic seasonality and nonlinear density-dependent factors regulate population size in an African rodent. Nature **389**:176–180.
Lin, C. C., and G. S. Mudholkar. 1980. A simple test for normality against asymmetric alternatives. Biometrika **67**: 455–461.
Logan, J. A., and F. P. Hain, editors. 1991. Chaos and insect ecology. Virginia Experiment Station Information Series 91-3. Virginia Polytechnic Institute and State University, Blacksburg, Virginia, USA.
May, R. M. 1974*a*. Biological populations with nonoverlapping generations: stable points, stable cycles, and chaos. Science **186**:645–647.
May, R. M. 1974*b*. Stability and complexity in model ecosystems. Second edition. Princeton University Press, Princeton, New Jersey, USA.
May, R. M., and G. F. Oster. 1976. Bifurcations and dynamic complexity in simple ecological models. American Naturalist **110**:573–599.
McCaffrey, D. F., S. Ellner, A. R. Gallant, and D. W. Nychka. 1992. Estimating the Lyapunov exponent of a chaotic system with nonparametric regression. Journal of the American Statistical Association **87**:682–695.
Miramontes, O., and P. Rohani. 1998. Intrinsically generated coloured noise in laboratory insect populations. Proceedings of the Royal Society of London **B265**:785–792.
Nychka, D. S., S. Ellner, D. McCaffery, and A. R. Gallant. 1992. Finding chaos in noisy systems. Journal of the Royal Statistical Society **B54**:399–426.
Olsen, L. F., and W. M. Schaffer. 1990. Chaos vs. noisy periodicity: alternative hypotheses for childhood epidemics. Science **249**:499–504.
Olsen, L. F., G. L. Truty, and W. M. Schaffer. 1988. Oscillations and chaos in epidemics: a nonlinear dynamic study of six childhood diseases in Copenhagen, Denmark. Theoretical Population Biology **33**:344–370.
Park, T., D. B. Mertz, W. Grodzinski, and T. Prus. 1965. Cannibalistic predation in populations of flour beetles. Physiological Zoology **38**:289–321.
Perry, J. N., I. P. Woiwod, R. H. Smith, and D. Morse. 1997. Estimating chaos in an insect population. Science **276**: 1881–1882.
Pool, R. 1989*a*. Is it chaos, or is it just noise? Science **243**: 25–28.
Pool, R. 1989*b*. Ecologists flirt with chaos. Science **243**:310–313.
Press, W. H., S. A. Teukolsky, W. T. Vetterling, and B. P. Flannery. 1992. Numerical recipes in FORTRAN: the art of scientific computing. Cambridge University Press, Cambridge, UK.
Rand, D. A., and H. B. Wilson. 1991. Chaotic stochasticity: a ubiquitous source of unpredictability in epidemics. Proceedings of the Royal Society of London **B246**:179–184.
Rao, C. R. 1973. Linear statistical inference and its applications. Second edition. John Wiley & Sons, New York, New York, USA.
Renshaw, E. 1994. Chaos in biometry. IMA Journal of Mathematics Applied in Medicine & Biology **11**:17–44.
Rice, J. A. 1995. Mathematical statistics and data analysis. Second edition. Wadsworth, Belmont, California, USA.
Rohani, P., and D. J. D. Earn. 1997. Chaos in a cup of flour. Trends in Ecology & Evolution **12**:171.
Rohani, P., and O. Miramontes. 1996. Chaos or quasiperiodicity in laboratory insect populations? Journal of Animal Ecology **65**:847–849.
Rothery, P., I. Newton, L. Dale, and T. Wesolowski. 1997. Testing for density dependence allowing for weather effects. Oecologia **112**:518–523.
Schaffer, W. M. 1984. Stretching and folding in lynx fur returns: Evidence for a strange attractor in nature? American Naturalist **124**:798–820.
Shaffer, M. L. 1981. Minimum population sizes for species conservation. BioScience **31**:131–134.
Simberloff, D. 1988. The contribution of population and community ecology to conservation science. Annual Review of Ecology and Systematics **19**:473–511.
Stenseth, N. C., O. N. Bjornstad, and T. Saitoh. 1996. A gradient from stable to cyclic populations of *Clethrionomys rufocanus* in Hokkaido, Japan. Proceedings of the Royal Society of London **B263**:1117–1126.
Tilman, D., and D. Wedin. 1991. Oscillations and chaos in the dynamics of a perennial grass. Nature **353**:653–655.
Tong, H. 1990. Nonlinear time series: a dynamical systems approach. Oxford University Press, Oxford, UK.
Turchin, P. 1993. Chaos and stability in rodent population dynamics: evidence from nonlinear time-series analysis. Oikos **68**:167–172.
Turchin, P. 1995. Chaos in microtine populations. Proceedings of the Royal Society of London **B262**:357–361.
Turchin, P., and A. D. Taylor. 1992. Complex dynamics in ecological time series. Ecology **73**:289–305.
Woiwod, I. P., and I. Hanski. 1992. Patterns of density dependence in moths and aphids. Journal of Animal Ecology **61**:619–629.
Zimmer, C. 1999. Life after chaos. Science **284**:83–86.

APPENDIX

Here we describe our numerical methods for the computation of the deterministic and stochastic Liapunov exponents for the LPA model. The calculations center around a times series of triples (L_t, P_t, A_t) and a matrix function $\mathbf{J}_t$ (Eq. 13). In the case of the Liapunov exponent (LE) the triples are a trajectory from the deterministic skeleton. In the case of the stochastic LE (SLE) the triples are a trajectory from the full stochastic model.

One problem with the direct use of Eq. 14 is that the matrix product may be unstable. A workaround is to ''scale'' the matrix product at each iteration. Let, $s_1, s_2, \ldots, s_t$ represent a set of positive scalars and let $\mathbf{S}_t = \mathbf{J}_t/s_t$. Then, from Eq. 14,

$$\lambda_t = t^{-1}\ln\|s_t s_{t-1}\cdots s_1 \mathbf{S}_t\mathbf{S}_{t-1}\cdots\mathbf{S}_1\| = t^{-1}\ln\|\mathbf{S}_t\mathbf{S}_{t-1}\cdots\mathbf{S}_1\| + t^{-1}\sum_{i=1}^{t}\ln s_i. \quad \text{(A.1)}$$

The ''trick'' is to choose the s_t scalars so that the matrix product remains stable. We used

$$s_t = \|\mathbf{J}_t\mathbf{S}_{t-1}\mathbf{S}_{t-2}\cdots\mathbf{S}_1\| \quad \text{(A.2)}$$

with $s_1 = \|\mathbf{J}_1\|$. With this definition, $\|\mathbf{S}_t\mathbf{S}_{t-1}\cdots\mathbf{S}_1\| = 1$, and from Eq. A1 we have

$$\lambda_t = t^{-1}\sum_{i=1}^{t}\ln s_i. \quad \text{(A.3)}$$

The Liapunov exponent can now be computed as an arithmetic mean of a sequence of scalars. At each iteration the Jacobian $\mathbf{J}_t$ is computed from the values of (L_t, P_t, A_t) and multiplied with the scaled matrix product $\mathbf{S}_{t-1}\mathbf{S}_{t-2}\cdots\mathbf{S}_1$, and the new scalar s_t is obtained as the norm of the matrix product $\mathbf{J}_t\mathbf{S}_{t-1}\mathbf{S}_{t-2}\cdots\mathbf{S}_1$. The matrix product $\mathbf{J}_t\mathbf{S}_{t-1}\mathbf{S}_{t-2}\cdots\mathbf{S}_1$ is divided by s_t to obtain a new scaled matrix product $\mathbf{S}_t\mathbf{S}_{t-1}\cdots\mathbf{S}_1$. Since, at each iteration, the norm of the scaled matrix product equals 1, the matrix product remains stable.

The problem of numerical roundoff error must also be handled carefully. At each iteration one must recompute the average Eq. A3 using the next scalar in the sequence. As t gets large, one must add a large number, the sum of the previous $t-1$ scalars, to a much smaller number, s_t. This can produce a large roundoff error. This loss of accuracy accumulates with each iteration.

A related problem is deciding on convergence. How large a value of t must one use in Eq. A3 to approximate Eq. 15 reasonably? Ideally, one would like to check for convergence within some error tolerance level at each iteration. However, as t gets large, adding another scalar to the mean does not have much effect on the mean. For example, the mean of $t = 1\,000\,000$ scalars will not be much different from the mean of $t = 1\,000\,001$ scalars, and it will look as if the mean λ has converged.

We addressed the roundoff problem by implementing an algorithm where the average Eq. A3 is built up from a series of averages of subsequences of scalars. For example, the average λ_4 is obtained as the average of $(s_1 + s_2)/2$ and $(s_3 + s_4)/2$. The average for λ_8 is obtained as the average of λ_4 and average of $(s_5 + s_6)/2$ and $(s_7 + s_8)/2$. To get λ_{16}, an average for $t = 9, \ldots, 16$ is computed in the same way λ_8 was computed and the averages for $t = 1, \ldots, 8$ and $t = 9, \ldots, 16$ are averaged. This process is repeated to get estimates λ_2, λ_4, λ_8, λ_{16}, λ_{32}, etc. At every step in the process, averages only occur between numbers computed from subsequences of the same length. All computations were done using double precision in the programming language C++ on a 32-bit operating system.

This algorithm also provides a conservative method for deciding on whether or not the average of the sequence has converged. The estimate of λ for $t = 1, \ldots, 2^n$ is obtained by averaging the mean of the subsequence for $t = 1, \ldots, 2^{n-1}$ and the mean of the subsequence for $t = 2^{n-1} + 1, \ldots, 2^n$. To decide on convergence, these two ''subsequence means'' are compared. If the absolute value of their difference is less than a certain error tolerance ε, then it is decided that convergence has occurred.

We have found that one must choose ε conservatively, especially for the SLEs. This is because one is computing λ from a single realization of the stochastic process. Although the process is ergodic, variation still occurs among SLEs estimated from finite sequences. We always repeat the estimation procedure using a different random-number sequence and compare estimates to make certain they agree.

Convergence occurs more quickly if one ''tosses out'' an initial subsequence of s_i's from the computation of the mean. This is because the scaled matrix product $\mathbf{S}_t\mathbf{S}_{t-1}\cdots\mathbf{S}_1$ tends to ''settle down'' as t gets large.

In the special case of a periodic attractor, the deterministic LE can be computed quickly and accurately without using the sequence-averaging method. Assume the deterministic process approaches a cycle with fixed period n. For large, t, $(L_t, P_t, A_t) = (L_{t+n}, P_{t+n}, A_{t+n})$. From Eq. 14 we can write, for $t = mn$,

$$\lambda_{mn} = (mn)^{-1}\ln\|(\mathbf{J}_{mn}\mathbf{J}_{mn-1}\cdots\mathbf{J}_{mn-n+1})\cdots(\mathbf{J}_n\mathbf{J}_{n-1}\cdots\mathbf{J}_1)\| = (mn)^{-1}\ln\|\mathbf{C}_m\cdots\mathbf{C}_1\|. \quad \text{(A.4)}$$

The matrices $\mathbf{C}_1, \mathbf{C}_2, \ldots, \mathbf{C}_m$, represent the product of the Jacobian matrices taken in groups of n. As the system converges onto its period-n cycle, the matrix $\mathbf{C}_m$ will approach a constant value $\mathbf{C}^*$, which is the product of the Jacobian matrices evaluated at each point on the cycle in the order in which they are visited. As $m \to \infty$, $t \to \infty$ and $\mathbf{C}_m \to \mathbf{C}^*$. Therefore, for large values of m, the matrix product $\mathbf{C}_m\mathbf{C}_{m-1}\cdots\mathbf{C}_1$ will approach asymptotically the value $\phi^m\mathbf{M}$, where ϕ is the largest modulus of the eigenvalues of $\mathbf{C}^*$ and $\mathbf{M}$ is a matrix of constants. From Eq. 15 we have

$$\lambda = \lim_{m\to\infty}\lambda_{mn} = \lim_{m\to\infty}(mn)^{-1}\ln\|\phi^m\mathbf{M}\| = \lim_{m\to\infty}(mn)^{-1}(m\ln\phi + \ln\|\mathbf{M}\|) = n^{-1}\ln\phi + \lim_{m\to\infty}(mn)^{-1}\ln\|\mathbf{M}\| = n^{-1}\ln\phi. \quad \text{(A.5)}$$

The LE can be computed directly from the eigenvalues of the matrix $\mathbf{C}^*$. The matrix $\mathbf{C}^*$ can be obtained by iterating the system until it converges to its stable n-cycle. Then the Jacobian matrices $\mathbf{J}_{t+1}, \mathbf{J}_{t+2}, \cdots, \mathbf{J}_{t+n}$ are computed and the product $\mathbf{C}^* = \mathbf{J}_{t+n}, \mathbf{J}_{t+n-1}, \cdots, \mathbf{J}_{t+1}$ is obtained. Next the eigenvalues of $\mathbf{C}^*$ are computed using one of the many numerical algorithms designed for this purpose. The LE is simply the logarithm of the largest modulus of the eigenvalues divided by the period.

In practice, we used the following procedure. We iterated the model 50 000 times to remove transients. Then we computed the scaled Jacobian product and generated the s_i scalars. If the model was deterministic, we tested for a cycle of period $n \le 100$. If a cycle was found, the average of n of the s_i's was the estimate of λ. If the model was stochastic or no cycle was detected, we tossed out the first 50 000 s_i's and used the ''subsequence averaging'' procedure described above on subsequent values of s_i to generate an estimate of λ.

Estimates of the deterministic LEs were usually obtained quickly. Convergence was much slower for the stochastic LEs; for example, for $\varepsilon = 0.0001$, convergence sometimes took over a million iterations. But convergence did occur in a consistent and repeatable fashion.